TOPICAL REVIEW

Physics and biology of ultrahigh dose-rate (FLASH) radiotherapy: a topical review

To cite this article: Nolan Esplen *et al* 2020 *Phys. Med. Biol.* **65** 23TR03

IOP Publishing Phys. Med. Biol. 65 (2020) 23TR03 https://doi.org/10.1088/1361-6560/abaa28

Physics in Medicine & Biology

IPEM Institute of Physics and Engineering in Medicine

TOPICAL REVIEW

Physics and biology of ultrahigh dose-rate (FLASH) radiotherapy: a topical review

RECEIVED
26 January 2020

REVISED
23 July 2020

ACCEPTED FOR PUBLICATION
28 July 2020

PUBLISHED
1 December 2020

Nolan Esplen[1], **Marc S Mendonca**[2] **and Magdalena Bazalova-Carter**[1]

[1] Department of Physics and Astronomy, University of Victoria, Victoria, BC, Canada
[2] Departments of Radiation Oncology & Medical and Molecular Genetics, Indiana University, Indiana University School of Medicine, IUPUI, Indianapolis, IN, United States of America

E-mail: bazalova@uvic.ca

Keywords: FLASH, ultrahigh dose-rate, radiobiology, dosimetry

Abstract

Ultrahigh dose-rate radiotherapy (RT), or 'FLASH' therapy, has gained significant momentum following various *in vivo* studies published since 2014 which have demonstrated a reduction in normal tissue toxicity and similar tumor control for FLASH-RT when compared with conventional dose-rate RT. Subsequent studies have sought to investigate the potential for FLASH normal tissue protection and the literature has been since been inundated with publications on FLASH therapies. Today, FLASH-RT is considered by some as having the potential to 'revolutionize radiotherapy'. FLASH-RT is considered by some as having the potential to 'revolutionize radiotherapy'.

The goal of this review article is to present the current state of this intriguing RT technique and to review existing publications on FLASH-RT in terms of its physical and biological aspects. In the physics section, the current landscape of ultrahigh dose-rate radiation delivery and dosimetry is presented. Specifically, electron, photon and proton radiation sources capable of delivering ultrahigh dose-rates along with their beam delivery parameters are thoroughly discussed. Additionally, the benefits and drawbacks of radiation detectors suitable for dosimetry in FLASH-RT are presented. The biology section comprises a summary of pioneering *in vitro* ultrahigh dose-rate studies performed in the 1960s and early 1970s and continues with a summary of the recent literature investigating normal and tumor tissue responses in electron, photon and proton beams. The section is concluded with possible mechanistic explanations of the FLASH normal-tissue protection effect (FLASH effect). Finally, challenges associated with clinical translation of FLASH-RT and its future prospects are critically discussed; specifically, proposed treatment machines and publications on treatment planning for FLASH-RT are reviewed.

1. Introduction

'I saw a FLASH brighter than a thousand suns,' reportedly said a PhD student Anatoli Bugorski whose head was accidentally irradiated by a 76 GeV proton pencil beam to a dose of 2–3 kGy during a malfunction of the Synchrotron U-70 in Protvino, Soviet Union in 1978. Mr. Bugorski suffered some radiation side effects, such as mental fatigue and loss of hearing in his left ear, but ultimately survived the incident and completed his PhD (Cottrell 2018). Based on existing knowledge of the biological effects of radiation at the time, this was an unexpected outcome given that receipt of such high radiation dose, albeit to a small volume, was considered lethal. The incident would seem to indicate that we did not have a full understanding of the radiobiological effects of ultra-short, ultrahigh dose-rate—'FLASH'—irradiations, which may, in light of modern research, provide a novel means for reducing the normal tissue side-effects following radiation treatment.

External beam radiation therapy (RT), dating back to the 1950s, is typically delivered with medical linear accelerators (linacs) and prior to the implementation of the flattening filter free (FFF) mode, the dose rates delivered to patients were limited to approximately 6 Gy min^{-1}. Population-based tumor control probability (TCP) and normal tissue complication probability (NTCP) models have since been derived from the

Table 1. Terminology used throughout the text.

Term	Symbol	Description
intra-pulse dose-rate	—	The duration of a single pulse.[a]
	$\bar{\dot{D}}$	Mean dose-rate for a multi-pulse delivery.
pulse repetition frequency	$\dot{D}_P$	Dose-rate in a single pulse.[a]
	DPP	Dose in a single pulse.[a]
	PRF	Number of pulses delivered per unit time.[a]
	t_i	Total irradiation time from the beginning of the first delivered pulse to the end of the last delivered pulse.
ultrahigh dose-rate	—	Radiation delivered with mean dose-rate of > ~ 40 Gy s^{-1}.
	—	Ultrahigh dose-rate RT that presents decreased damage to normal tissues compared to RT delivered with conventional dose–rate of ~0.04 Gy s^{-1}.

[a]Pulses are considered to be macro-pulses unless otherwise stated (see also figure 1).

[b]In literature sometimes referred to as the instantaneous dose-rate.

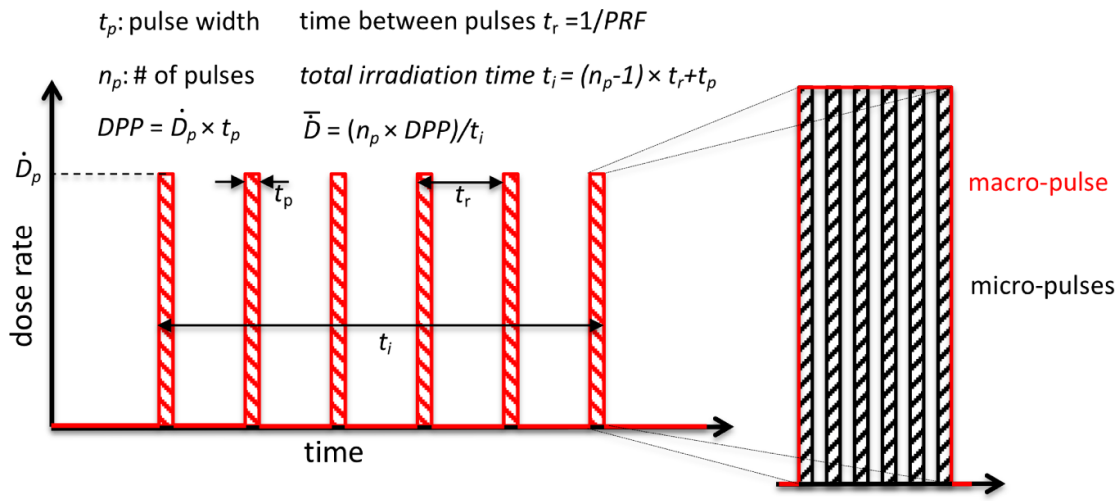

Figure 1. Schematics of pulsed beam temporal structure.

extensive outcomes data available for patients treated on these linacs. In 2014, however, Favaudon *et al* used a mouse model to demonstrate that using an ultrahigh dose-rate (>40 Gy s^{-1}) beam could result in a reduction in NTCP while maintaining TCP when compared with conventional dose-rate RT (Favaudon *et al* 2014). Their work rekindled much interest in the application of ultrahigh dose-rate RT (Maxim *et al* 2019a), which has resulted in many subsequent publications on the topic. In this review article arising from the authors' presentations at the 2019 Winter Institute of Medical Physics (WIMP), we build on existing FLASH review articles (Durante *et al* 2018, Kamperis *et al* 2019, Wilson *et al* 2020) and summarize past and recent science of ultrahigh dose-rate FLASH-RT in terms of radiation sources, dosimetry and biology while presenting possible avenues for clinical translation of FLASH-RT.

For the reader's convenience, table 1 summarizes the terminology used throughout the topical review.

2. Physics

2.1. Radiation sources

The delivery of FLASH-RT has previously been characterized by irradiation at ultrahigh mean dose-rates (>40 Gy s^{-1}) to effect single sub-second treatment fractions (Favaudon *et al* 2014, Montay-Gruel *et al* 2017, Vozenin *et al* 2019a). However, because the physical beam parameters required to drive the normal tissue sparing remain to be elucidated, this 40 Gy s^{-1} dose-rate definition is currently in flux. In particular, inter-dependent temporal parameters (figure 1), such as the dose per pulse (DPP), intra-pulse dose-rate ($\dot{D}_P$), pulse repetition frequency (PRF), as well as mean dose rate ($\bar{\dot{D}}$) and the total irradiation time may each be of particular importance (Simmons *et al* 2019, Bourhis *et al* 2019a). The role of such parameters must be explored to determine the source requirements for safe exploitation of FLASH-RT and optimization of the potential therapeutic benefit.

Unfortunately, while there is an immediate need to identify the beam-related requirements for FLASH-RT, there are few systems available worldwide which are capable of reaching the requisite dose rates. Furthermore, given that the influence of the beam time-structure is as of yet unclear, prospective irradiators would ideally accommodate a large range of temporal parameters in order to enable systematic exploration of the pulsed beam structure.

To date, the FLASH effect has been most commonly demonstrated using low-energy electron linacs (Vozenin *et al* 2019b). However, in an attempt to rapidly address the outstanding questions associated with FLASH-RT, existing technologies are being retrofitted (Schüler *et al* 2017b, Montay-Gruel *et al* 2018, Lempart *et al* 2019, Bazalova-Carter and Esplen 2019), and new technologies developed (Patriarca *et al* 2018, Esplen *et al* 2019, Maxim *et al* 2019b) in order to improve the availability of ultrahigh dose-rate sources. Additionally, FLASH-RT is being expanded to other treatment modalities that may be better suited to the treatment of deep-seated tumors, and includes very high-energy electrons (VHEE), megavoltage (MV) x-rays as well as protons, possibly combined with intensity-modulation.

In the forthcoming discussion, an overview of the currently available and prospective FLASH-RT sources, including those suited for investigations into biological effects of ultrahigh dose-rates, is presented.

2.1.1. Electron sources

Experimental and medical electron accelerators continue to represent valuable, and comparatively affordable, options for delivering ultrahigh dose-rate RT, but the different capabilities between accelerators necessitates careful consideration of the specific qualities which will enable their use in FLASH-RT contexts. Insight into these qualities may be gleaned from an examination of accelerators, which have been, or may potentially be, employed in the delivery of FLASH-RT.

The normal tissue sparing potential of ultrahigh dose-rate irradiation was first demonstrated using electron linacs in a number of radiobiological studies over the past 40 years (see section 3.1). Since then, the concept of ultrahigh dose-rate RT has been re-established, based on exploitation of an observed differential effect between tumor and normal tissue, through the use of sophisticated new accelerators capable of delivering pulsed beams with a wide variety of temporal configurations. Today, the Kinetron and Oriatron eRT6 electron linacs are among the most recognizable FLASH irradiators in the current literature, having been used at Orsay and Lausanne University Hospital, respectively, for the successful *in vivo* treatments of small-animal models, veterinary cases and a treatment of one patient (Bourhis *et al* 2019b).

2.1.1.1. FLASH-RT capable sources

The Kinetron (CGR-MeV, Paris, France) delivers a pulsed electron beam with a beam energy of 4–5 MeV and can be operated in conventional ($\overline{\dot{D}}$<0.03 Gy s^{-1}, DPP ~ 10^{-3} Gy) or 'FLASH' irradiation modes ($\dot{D}_P$>2 × 10^7 Gy s^{-1}, DPP ⩾ 1 Gy) with a pulse output reproducibility better than 5% (Favaudon *et al* 1990, 2014, Lansonneur *et al* 2019). The accelerator, driven by an adjustable triode electron gun, can provide beam currents between 10–250 mA (based on variable grid tension), pulse widths between 0.1–2.2 μs (in FLASH mode) and macro-pulse *PRF*s of 10–250 Hz (Favaudon *et al* 1990, Lansonneur *et al* 2019). This flexibility enables the linac to achieve $\overline{\dot{D}}$ between 10^{-1} and 10^3 Gy s^{-1} under typical treatment conditions.

The Oriatron eRT6 (PMB, Peynier, France) is another experimental electron linac, similar to the Kinetron that preceded it, which allows output control based on fine control over a number of beam parameters of interest, including the number of electron pulses, PRF (5–200 Hz), pulse width (0.5–2.2 μs), and the triode electron gun grid tension (0–300 V), which drives a peak beam current of up to 300 mA with a mean value of 30 μA. The eRT6 beam energy is nominally between 4.9–6 MeV, depending on the dose-rate, and can be tuned to achieve a $\dot{D}_P$ which is a factor of 10^4 greater than conventional linacs, albeit with comparable PRFs and pulse widths (Petersson *et al* 2017, Jaccard *et al* 2018). For example, Petersson *et al* (2017) achieved $\overline{\dot{D}}$ on the order of 10^{-2} Gy s^{-1}and 10^3 Gy s^{-1}, corresponding to $\dot{D}_P$ between 10^2 Gy s^{-1}and 10^7 Gy s^{-1}, and a DPP between 10^{-4} Gy and 10^1 Gy, assuming a pulse width and PRF of 1.8 μs and 100 Hz, respectively. Importantly, the eRT6 boasts the capacity to deliver ultrahigh dose-rates at standard 100 cm source-to-surface distances (SSD) using a field size of 1.6–20 cm and has a therapeutic (R_{80}) range between 1.8 cm and 2.3 cm (Jaccard *et al* 2018). Recent studies with the eRT6 have demonstrated a reproducible FLASH effect through the use of a pulsed beam comprising 1–10 pulses (1.8–2 μs width) delivered in <200 ms, and $\dot{D}_P$ > 1.8 × 10^5 Gy s^{-1} (Bourhis *et al* 2019a).

While they differ in beam qualities and peak performances, the Kinetron and Oriatron eRT6 both use a micro pulse structure superimposed by millisecond macro pulses, which themselves feature a $\dot{D}_P$ on the order of 10^6 Gy s^{-1} (Favaudon *et al* 2014, Jaccard *et al* 2018, Lansonneur *et al* 2019). This provides an important temporal similarity between the pulsed beams of the two linacs beyond simply their capacity to deliver ultrahigh dose-rates.

In a bid to improve accessibility of sources with which ultrahigh dose-rates may be delivered, there has been a recent effort to adapt existing clinical linacs for electron FLASH-RT experiments (Schüler *et al* 2017b, Lempart *et al* 2019). Such modified linacs have been successfully employed to deliver electron beams with $\overline{\dot{D}}$ exceeding 200 Gy s^{-1}, so as to be compatible with the early definition for FLASH ($\overline{\dot{D}} > 40$ Gy s^{-1}), however, their dosimetric and geometric properties, namely small field sizes at very short SSD (within treatment head), are suitable only for small-animal experiments. Lempart *et al* (2019), demonstrated a scheme to achieve $\overline{\dot{D}}$ between 30–300 Gy s^{-1} (DPP = 0.1–1.9 Gy; PRF = 200 Hz) on an Elekta Precise linac (E ~ 8 MeV), depending on measurement point within the treatment head. Schüler *et al* (2017b) were similarly successful in delivering ultrahigh dose-rates using a modified Varian Clinac 21EX, although initially only at the location of the ion chamber (achieving $\overline{\dot{D}} = 74$ Gy s^{-1} at 1 cm depth) and with the 9 MeV beam at a beam current of 400 nA. By using a subsequently more intensive linac tuning procedure, a 13- and 40-fold increase in dose rate was observed for the 9 MeV (110 nA) and 20 MeV (400 nA) beams, respectively. In this tuned configuration, $\overline{\dot{D}}$ was measured to be 220 Gy s^{-1} ($\dot{D}_P = 1.7 \times 10^6$ Gy s^{-1} at 1 cm depth) at the location of the mirror, chosen so that depth-dose and field size characteristics remained suitable for small-animal experiments.

Relative to the Kinetron and eRT6, the higher mean energy (~8–20 MeV) of electrons delivered with these sources had the added benefit of reduced depth-dose falloff resulting in improved dose homogeneity in small-animal FLASH-RT, although there is inevitably a reduced flexibility in treatment setup and parameter selection. Both groups found that higher dose rates were generally achieved at the expense of field homogeneity and field size, as might be achieved through thinning or removal of the scattering foils. The modified linac of Schüler *et al* (2017b) was used in a study by Simmons *et al* (2019) who isolated the total delivery time as the temporal parameter of interest and maintained 2 μs pulses with DPP = 1.75 Gy and $\dot{D}_P = 8.75 \times 10^5$ Gy s^{-1}. $\overline{\dot{D}}$ for FLASH treatments, either 200 Gy s^{-1} or 300 Gy s^{-1} for 20 MeV and 16 MeV beams, respectively, were therefore modulated by the PRF which were set, correspondingly, to 108 Hz or 180 Hz.

2.1.1.2. Prospective sources

2.1.1.2.1. Linear accelerators

High-energy research accelerators are proving to be highly attractive for their ability to provide access to a range of beam parameters beyond dose rate and DPP. For example, the Electron Linac of high Brilliance and low Emittance (ELBE) at Helmholtz-Zentrum Dresden Rossendorf (HZDR, Dresden, Germany) and the high-power electron linac of the Advanced Rare Isotope Laboratory (ARIEL) facility at TRIUMF (Vancouver, BC, Canada) as well as the Next Linear Collider Test Accelerator (NLCTA) at SLAC National Acceleator Laboratory (Stanford, CA, USA) represent promising candidates in this regard. Each of these accelerators might allow for research into the effects of temporal parameters beyond those that can be achieved with the above-mentioned electron linacs, including *PRF*, pulse width, beam current and pulse sequence over a much broader range.

The ELBE is designed to deliver pulsed electron beams with energies up to 40 MeV, using 5 ps micro-pulses with charge up to ~70 pC at quasi-continuous (i.e. with 13 MHz nominal micro-pulse PRF) beam currents of up to ~1 mA (Michel *et al* 2006, Karsch *et al* 2012). The micro-pulse DPP is 60 mGy and the quasi-continuous (CW) beam can be further modulated by superimposing a macro-pulse structure with 0.1–40 ms macro-pulse widths or by using a finite number (<4096) of micro-pulses in a single-pulse mode. [3] With relevance to FLASH-RT, the accelerator has been used previously by Karsch *et al* (2012) in the evaluation of the dose-rate dependence for various dosimeters at ultrahigh dose-rates, by Gotz *et al* (2017) in the validation of ionization chamber (IC) saturation models suitable for arbitrarily high DPP and PRF delivery, and appears well-suited for application in ultrahigh dose-rate contexts where pulsed radiation is desired. The ELBE high $\dot{D}_P = 10^9$–10^{10} Gy s^{-1} (Beyreuther *et al* 2015) should make it suitable for adoption as an experimental source in future FLASH radiobiological studies. Specifically, as the mean dose-rate is driven by the beam time structure, a sufficiently high micro-pulse PRF along with appropriate macro-pulse widths or CW operation will enable ultrahigh mean dose-rates to be achieved in the desired sub-second intervals. For a single ~4 μs macro pulse, for example, a DPP of >3 Gy may be achieved using the 70 pC (60 mGy) micro-pulses at 13 MHz PRF.

Similarly, the ARIEL e-linac at TRIUMF (Vancouver, BC, Canada) is currently being adapted for ultrahigh dose-rate delivery and may eventually accelerate electrons with energy up to 30 MeV for *in vivo* studies. At 10 MeV, the e-linac delivers a quasi-continuous beam with a power of 10 kW, maximum *PRF* of 10 kHz and the duty cycle can set arbitrarily down to a minimum of 1%, which corresponds to a *PRF* of

[3] www.hzdr.de/db/Cms?pOid=40450&pNid=0&pLang=en.

10 Hz (Planche 2019). The expected $\bar{\dot{D}}$ for a 10 MeV continuous electron beam is >1000 Gy s^{-1}, based on the increased dose-per-electron compared to dose-per-photon and the Bremsstrahlung efficiency of the photon system currently under development (Esplen *et al* 2019).

The SLAC NLCTA is a high-brightness electron linac, which has been employed for investigations into the use of very-high energy electrons (VHEE) for rapid treatment (at high dose-rate) of deep-seated tumors (Bazalova-Carter *et al* 2015a, 2015b, Palma *et al* 2016, Schüler *et al* 2017a). The NLCTA beamline delivers 60–120 MeV VHEE beams with a pulse width of 1 ps and maximum PRF of 10 Hz, resulting in $\bar{\dot{D}} = 90$ Gy s^{-1} for a 60 MeV beam (Bazalova-Carter *et al* 2015a). Owing to the limited dose deposition over sub-second time frames of interest in FLASH-RT, the NLCTA beamline may be best suited for studies on the lower-dose FLASH effect threshold or those associated with radiosensitive tumor cell lines.

While VHEE electron treatments might be possible with future improvements to laser-accelerators (discussed below) or research accelerators (i.e. TRIUMF or ELBE), the fixed beamlines in question are only suited to preclinical treatments owing to the lack of a gantry-mounted or electromagnetic steering solution. One solution for realizing multi-directional electron FLASH treatments is the Stanford Pluridirectional High-energy Agile Scanning Electronic Radiotherapy (PHASER) (Maxim *et al* 2019b), which is described in greater detail in section 4.1. Of particular relevance to electron FLASH sources, the system will leverage compact, high-gradient (100 MeV m^{-1} with pulse compression) DRAGON linear accelerators which are capable of providing an enhanced RF-to-beam conversion efficiency, and thus a high duty factor. This, along with a high charge-per-pulse, can help facilitate a 300-fold increase in beam current when compared to conventional systems which will help to drive ultrahigh dose-rate irradiations with electron energies >100 MeV.

2.1.1.2.2. Laser plasma accelerators

Of future relevance to ultrahigh dose-rate electron therapies is the maturation of compact accelerator technologies capable of high accelerating gradients (on the order of 100 GeV m^{-1}) based on laser-plasma (wakefield) acceleration (Tajima *et al* 2004). Modern laser-plasma electron accelerators are notable for their high $\dot{D}_P$ (~10^9–10^{11} times greater than conventional linacs) (Beyreuther *et al* 2010) and the capacity to accelerate stable, quasi-monoenergetic beams of low- to very-high energy electrons (10–250 MeV) (Geddes *et al* 2004, Faure *et al* 2004, 2006, Mangles *et al* 2004, Glinec *et al* 2005), and therefore eventually serve as viable solutions for achieving clinical VHEE FLASH beams (Glinec *et al* 2006, Malka *et al* 2008). A pre-requisite for this laser-acceleration modality is the use high power (tera- or peta-watt) lasers, made possible by chirped pulse amplification (Strickland and Mourou 1985, Maine *et al* 1988) and ultra-short <100 fs pulses (Glinec *et al* 2005, Beyreuther *et al* 2010, Karsch *et al* 2017).

While stable beams are usually driven at low 10 Hz *PRF*s, kHz frequencies have been achieved at the Laboratoire d'Optique Appliquee (LOA) (Palaiseau, France) with the '*salle jaune*' laser (Pittman *et al* 2002) using lower energy 2.1–2.5 mJ, <4 fs laser pulses and micro-scale supersonic (N_2) gas jets (Guénot *et al* 2017, Gustas *et al* 2018). This new delivery scheme fostered a significant increase in the *PRF* and beam current. However, the mean energy (1–5 MeV) of this system and the individual bunch charge (<24 pC $bunch^{-1}$) were both reduced relative to that of Faure *et al* (2004) (>100 MeV, 0.5 nC $bunch^{-1}$). The resulting beams are currently only achieved with low beam currents, relative to conventional accelerators, with 24 nA being the highest reported as of 2018 by Gustas *et al*.

The feasibility of laser-accelerated electrons for RT has been considered previously (Kainz *et al* 2004, Chiu *et al* 2004, Rigaud *et al* 2010, Lundh *et al* 2012). Importantly, Glinec *et al* (2006) examined the use of laser-accelerated electrons for VHEE RT using scanned beams, or single pulse treatments with very-high maximum DPP of 10 Gy using a focused beam with the energy peaked at 170 MeV and operating at up to 10 Hz *PRF*. Due to the high DPP, being very near to the dose suitable for a single high-dose treatment fraction (~10 Gy to 15 Gy), and short ~30 fs bunch duration, such a source may be a future candidate for VHEE FLASH-RT. Improvements in *PRF* along with longer pulses or higher, combined with suitably high beam currents may foster increased utility of laser accelerators for FLASH radiobiological experiments in the future. Table 2 summarizes the discussed ultrahigh dose-rate electron sources.

2.1.2. Photon sources

2.1.2.1. FLASH-RT capable sources

To date, biological effects of photon FLASH-RT have been demonstrated using ultrahigh dose-rate x-ray beams generated at the European Synchrotron Research Facilities (ESRF, Grenoble, France). Therein, Montay-Gruel *et al* (2018) demonstrated normal-tissue sparing, via reduced cognitive defects, for whole brain irradiation of mice. The irradiations were performed at timescales of 0.27 s, using a field height of 17 mm and $\bar{\dot{D}}$ of 37 Gy s^{-1}, which were compatible with the electron FLASH treatments described, for example, by Vozenin *et al* (2019a) and Favaudon *et al* (2014). The authors delivered ~100 keV (mean energy)

Table 2. Summary of operational ultrahigh dose-rate electron sources and their peak operating parameters.

Source	Energy (MeV)[a]	Max current (mA)	$\overline{\dot{D}}$(Gy s^{-1})[b]	*PRF* (Hz)[d]	Ref.
Oriatron (eRT6)	4.9–6	300	3000	10–200	(Jaccard *et al* 2018)
Kinetron	4–5	250	1000	10–200	(Favaudon *et al* 2014)
ELBE[c]	5–40	1.6	10^6	$\leqslant 13 \times 10^6$	(Karsch *et al* 2012)
NLCTA	60–120	60 000[f]	90	10	(Bazalova-Carter *et al* 2015a)
Elekta Precise	~8	—	1000	200	(Lempart *et al* 2019)
Varian Clinac 21EX	9, 20	0.00011	900	180	(Schüler *et al* 2017b)
		> 0.0004[e]	900	108	

[a]Energies correspond to the nominal value or range of values quoted in the relevant literature.
[b]Dose-rate corresponds to the maximum value derived from literature.
[c]www.hzdr.de/db/Cms?pNid=584: current is quoted as the peak average value for the nominal 13 MHz micro-pulse PRF.
[d]Maximum tunable PRF: often the macro-pulse PRF except for research accelerators where micro-pulse parameters may also be adjustable.
[e]The 400 nA average current was reported for clinical settings using the 20 MeV beam. After linac tuning the beam current is expected to have increased.
[f]For single 1 ns long, 60 pC electron pulse.

quasi-continuous x-rays on the ID17 biomedical beamline of the third-generation 6 GeV synchrotron located at the ESRF with a scanned 50 μm microbeam which boasted an in-slice $\overline{\dot{D}}$ of 12 000 Gy s^{-1}. The beam of the ID17 is of very high-brilliance and capable of an extremely high photon fluence with quasi-monoenergetic quality and low divergence, properties which are common to synchrotron radiation. The $\overline{\dot{D}}$ achieved are extremely high, between 8000 Gy s^{-1} and 16 000 Gy s^{-1} (200 mA peak current; ~ 80 Gy s^{-1} mA^{-1}, PRF 355 MHz) (Serduc *et al* 2006, Bräuer-Krisch *et al* 2015); however, the field size is limited to 1–3 mm high by ~40 mm wide, and targets must be scanned to achieve homogenous coverage (Siegbahn *et al* 2009, Sabatasso *et al* 2011, Prezado *et al* 2012). The energy spectrum of the preclinical beam is nominally between 30–600 keV with a mean energy of ~105 keV (Laissue *et al* 2013, Crosbie *et al* 2015); for veterinary trials the energy is lowered to 100 keV with the output reduced to 40 Gy s^{-1} mA^{-1}. It is important to note that the radiobiological consequences of combining micro- or mini-beam spatial-fractionation, which presents its own normal tissue-sparing advantages, with FLASH-RT as well as the use of prolonged exposures and variable dose-rates, which may be encountered using scanned micro-beams or actively scanned pencil beams, each remain to be determined.

2.1.2.2. Prospective sources

Another synchrotron facility currently primed to deliver kilovoltage (kV) FLASH-RT is the Imaging and Medical Beamline (IMBL) of the Australian Synchrotron (Melbourne, Australia). In addition to delivering various synchrotron modalities, including broad-beam (SBBRT) and microbeam radiotherapy (MRT), it has recently been employed for ultrahigh dose-rate SBBRT (Smyth *et al* 2018). The IMBL is equipped with a 3 GeV storage ring that operates with an electron current of 200 mA (Fournier *et al* 2016) and PRF of 500 MHz (Dowd *et al* 2008). It is capable of delivering $\overline{\dot{D}}$ of up to 700 Gy s^{-1} at 2 cm depth in water over a small 0.5–2 mm high, 30 mm wide field (Livingstone *et al* 2016a). Measured in air, however, the dose rate may exceed 4000 Gy s^{-1} (Archer *et al* 2019). The mean energy of the beam for imaging and therapy applications is typically between 60–500 keV (Stevenson *et al* 2017) and the synchrotron runs in a 'top-up' mode which avoids a time-dependent decrease in beam current (Davis *et al* 2019). For scanned, SBBRT treatments used by Smyth *et al* (2018), the $\overline{\dot{D}}$ at a depth of 5 mm in water was only 37–41 Gy s^{-1} with mean energy of 124 keV and, while this was compatible with the FLASH definition at that time ($\overline{\dot{D}}$>40 Gy s^{-1}), no FLASH effect was observed. By contrast, the MRT dose rates employed by the same authors reached 276–319 Gy s^{-1}, with mean energy of 96 keV. According to Livingstone *et al* (2017), kGy s^{-1} dose-rates comparable to those of at the ESRF may be achieved at reference (2 cm) depths by increasing the wiggler field (to 4T) and changing the filtration, albeit at the expense of changing the energy spectrum.

Evidently, the IMBL bears similarities to the ESRF ID17 beamline and so the lack of a demonstrated FLASH effect may be related to experimental differences rather than former source's theoretical compatibility with FLASH-RT. For example, it is assumed that Smyth *et al* (2018) were required to use a far lower scanning speed compared to Montay-Gruel *et al* (2018) in order to achieve the quoted broad-beam dose rates (~40 Gy s^{-1}) in their study's SBBRT configuration. While the ESRF irradiation completed in 270 ms using a scanning speed 62 mm s^{-1}, the dosimetry results of Livingstone *et al* (2017) indicate a maximum scan speed of 20 mm s^{-1} which for a (30 × 30) mm mouse-head irradiation necessitates a >1 s total irradiation time.

Other synchrotron facilities around the world have reported on preclinical SBBRT, MRT, or minibeam RT (MBRT) treatments with peak dose-rates similarly exceeding 40 Gy s^{-1}. For example, at the 8 GeV Spring-8 BL28B2 beamline (Hyogo, Japan), a 140 Gy s^{-1} (air kerma rate) (Uyama *et al* 2011) and a mean energy of 90 keV are reached using a 100 mA stable electron current (Ohno *et al* 2008, Mukumoto *et al* 2017). The 2.8 GeV National Synchrotron Light Source x17B beamline at Brookhaven National Laboratory (Upton, New York) has also achieved dose rates up to 830 Gy s^{-1} (Dilmanian *et al* 2002) at a mean energy of 50–120 keV for a *PRF* of 53 Hz with 2 ns pulses (Slatkin *et al* 1995, Laissue *et al* 1998) while a 2×2 cm^2 broad-beam was delivered at a $\overline{\dot{D}}$ of 100 Gy s^{-1} (Dilmanian *et al* 2003). While promising, the use of synchrotron x-ray beams in FLASH experiments warrants further investigation since the inherently small field size requires the beam to be scanned across the extended treatment volume in order to achieve the desired 'broad beam' coverage. This has the effect of reducing $\overline{\dot{D}}$ to values which might compromise the overall treatment duration and, in turn, manifestation of the FLASH effect. Consequently, an important consideration in synchrotron FLASH-RT becomes whether the beam scanning time may be completed in a fraction of a second (i.e. ~10^2 ms), irrespective of the dose rates being employed.

Unfortunately, while synchrotron x-ray treatments are attractive for use in radiobiological research, kV x-rays are generally not well suited to the treatment of deep-seated tumors. The primary constraint derives from the limited beam penetration at these energies which effects a rapid reduction in the mean dose-rate with depth in tissue. However, by combining kV spatial-fractionated and intensity-modulated arc therapies (Breitkreutz *et al* 2019, Dilmanian *et al* 2019) with ultrahigh dose-rate deliveries, possibly via synchrotron-generated mini-beams or next-generation high-brilliance compact x-ray sources, it may be possible to enable kV photon FLASH-RT within larger subjects. Alternatively, the use of megavoltage (MV) photons could very readily address the above-mentioned limitations of kV x-rays. For example, the use of MV photons may improve maximum and OAR dose conformality owing to a reduced depth-dose dependency and the possibility for intensity-modulation within larger, clinically-relevant treatment volumes.

Assuming the requisite dose rates and temporal beam parameters can be achieved, MV photons become attractive alternatives to VHEE or low-energy electrons for ultrahigh dose-rate irradiation. New intensity-modulation techniques would need to be implemented, however, as traditional photon IMRT and arc treatment modalities require slow-moving (1 rot min^{-1}) gantries, which are not compatible with the sub-second treatments that characterize FLASH-RT. Nevertheless, the favorable depth-dose characteristics and reduced entrance doses remain as attractive characteristics for future volume optimization. Alike to the VHEE modality described in section 2.1.1.2, there exist technical challenges that must be met before practical MV photon FLASH treatments can be realized. In the case of bremsstrahlung target accelerators, for example, the required infrastructure must tolerate high instantaneous power deposited by the primary electron beam. Owing to limited Bremsstrahlung conversion efficiencies, achieving ultrahigh dose-rates requires much higher beam power when compared to the primary electron beam. Furthermore, extreme target temperatures are reached due to significant heat deposition (electron stopping) within the converter, which in turn restricts the target material selection (i.e. to high atomic number, high density refractory metals) and demands that thermo-mechanical stresses and cooling requirements are carefully evaluated. The SPHINX target design proposed for the PHASER system (section 4.1) presents an interesting solution, by leveraging a high thermal mass tungsten target which doubles as a photon collimator to simultaneously produce and modulate the photon field.

To establish a first experimental platform for FLASH-RT experiments with MV photons, the ARIEL e-linac housed at TRIUMF is being adapted to deliver a 1–10 kW, 10 MeV electron beam (0.1–1 mA beam current) that will be used to produce a horizontal 10 MV x-ray source. The driving electron beam shares the same temporal capabilities previously described for ARIEL (see section 2.1.1.2), while the x-ray beam will deliver mean dose-rates of >100 Gy s^{-1} by converting $\geqslant$1 kW of incident electron beam power. The associated *in vivo* experimental station will foster exploration of temporal and energy beam characteristics and related biological consequences of using an ultrahigh dose-rate photon beam. Of particular interest will be the ability to deliver both arbitrarily pulsed and continuous primary beams and the correspondingly large beam parameter space (Esplen *et al* 2019).

Alternative x-ray sources that are capable of ultrahigh dose-rates have been investigated in the literature, but remain primarily suited to radiobiological experiments. This includes high-brightness, laser-driven plasma x-ray sources (Kmetec *et al* 1992, Schnürer *et al* 1995, Tillman *et al* 1999, Hill *et al* 2002, Shinohara *et al* 2004), which are nominally capable of achieving $\dot{D}_P$ of the order 10^{11} Gy s^{-1}. For example, Shinohara *et al* (2004) employed a 20 TW, 500 fs ($I = \sim 10^8$ W cm^{-2}) pulsed laser at GEKKO MII (Osaka, Japan) to generate <1 ps x-ray pulses of $\dot{D}_P$ of 10^{12}–10^{13} Gy s^{-1} with energies between hundreds of kV to 1 MV. Unfortunately, the low PRFs limited by the driving laser, restrictive geometries, limited reproducibility and low <1 MeV photon energies disallow their use beyond radiobiological experiments. Conventional

Table 3. Summary of ultrahigh dose-rate photon sources and their selected operating parameters.

Source	Energy[a]	Max current (mA)	$\overline{\dot{D}}$(Gy s^{-1})[b]	*PRF* (MHz)[c]	Ref.
ESRF (ID17)	105 keV	200	16 000	355	(Crosbie *et al* 2015)
IMBL	94 keV	200	4000	500	(Archer *et al* 2019)
MXR 160/22	160 kVp	18.75	114	N/A	(Bazalova-Carter and Esplen 2019)

[a]For ESRF and IMBL synchrotron sources, the average energy for the preclinical radiotherapy spectra are reported. For the conventional x-ray tube, the peak tube voltage is used instead.

[b]The dose-rate corresponds to the maximum value derived from literature and, in the case of the synchrotron sources, is inclusive of in-slice microbeam dose-rates.

[c]The pulse-repetition-frequency (PRF) is here representative of the electron repetition frequency in the storage ring. In the case of the x-ray tube a shutter mechanism can provide pulsing, but its performance has not been benchmarked.

(Bazalova-Carter and Esplen 2019) and recently-proposed line-focus (Bartzsch and Oelfke 2017) x-ray tubes can also be made capable of reaching dose-rates in excess of 100 Gy s^{-1} either in close proximity or at a distance from the focal spot, respectively, and might offer more compact solutions for low-energy FLASH-RT experiments to be conducted. Bazalova and Esplen (2019) further proposed a fast-shutter system to allow for sub-second pulsed delivery of a continuous beam. The line focus source proposed by Bartzsch and Oelfke (2017), if successfully implemented, could also help to drive clinical translation of ultrahigh dose-rate MRT through the delivery of hard (up to 600 kVp) x-ray beams with an expected maximum $\overline{\dot{D}}$ of 180 Gy s^{-1} at 50 cm from the source.

Table 3 summarizes the discussed ultrahigh dose-rate photon sources.

2.1.3. Proton sources

Current proton therapy sources have been identified as potential platforms for clinical translation of FLASH-RT. For clinical radiation therapy, proton beams are usually accelerated using synchrotrons or cyclotrons to energies of up to 250 MeV, while the proton pencil beams are typically capable of delivering ultrahigh dose-rates. Small targets can be irradiated with existing proton machines with minor or no modifications (Diffenderfer *et al* 2020). More generally, however, the difficulty with proton FLASH-RT comes from the need to deliver ultrahigh dose-rate beamlets across an extended volume to generate the spread-out Bragg peak (SOBP), which itself might not experience sufficiently high mean dose-rates during the treatment. While there are no *in vivo* data for conformal FLASH irradiations, it is nevertheless reasonable to assume that ultrahigh dose-rates could be achieved in the plateau region and therefore that the FLASH effect might still be observed in the normal tissues therein.

2.1.3.1. FLASH-RT capable sources

The ProBeam system (Varian Medical Systems, Palo Alto, CA) uses an isochronous cyclotron with a frequency of 72 MHz that accelerates protons to energies up to 250 MeV with beam current of up to 800 nA. The plateau dose rate to a 2 × 2 cm^2 area irradiated by a scanned ~3 mm pencil beam is approximately $\overline{\dot{D}} = 240$ Gy s^{-1}, which is increased by a factor of ~3 in the Bragg peak (Abel 2019). The Varian ProBeam proton beam is typically delivered in quasi-continuous fashion; however, it can also be delivered with a pulse width of 4 μs and repetition rate of up to 2 kHz and an in-pulse beam current of up to 30 μA (Busold and Röcken 2017). These beam structure parameters result in estimated dose rates of $\dot{D}_P = 9 \times 10^3$ Gy s^{-1} and $\overline{\dot{D}} = 72$ Gy s^{-1}. The ProBeam system has recently been used for FLASH irradiations of lung tumors (Rama *et al* 2019) and healthy lung tissue (Girdhani *et al* 2019) with $\overline{\dot{D}} = 40$ Gy s^{-1}.

The Proteus proton therapy system (Ion Beam Applications S.A, Louvain-La-Neuve, Belgium) accelerates protons to energies up to 230 MeV. The beam current reaches 300 nA under normal clinical conditions, but can be increased to 500 nA for non-clinical applications (Bloch 2019). The IBA Proteus proton beams are accelerated using isochronous cyclotrons that deliver what are effectively continuous beams. The system has recently been used to deliver FLASH-RT using a doubly-scattered and collimated 230 MeV beam at a mean dose rate of 78.9 Gy s^{-1} to mice (Diffenderfer *et al* 2020). The system was also used to deliver ultrahigh dose rates to zebra fish embryos with $\overline{\dot{D}}$ of 100 Gy s^{-1} (Beyreuther *et al* 2019b) and has recently delivered a $\overline{\dot{D}}$ of ~200 Gy s^{-1} in the Bragg peak at UMCG in Groningen, The Netherlands. Researchers at UMCG demonstrated the ability to scan a (5 × 5 × 5) cm^3 volume with does reaching 24 Gy in 530 ms, corresponding to a mean dose rate of $\overline{\dot{D}} = 45$ Gy s^{-1}.[4] These dose rates were achieved by using a 300 nA passively scattered beam and with a ridge filter to achieve the desired SOBP.

[4] www.youtube.com/watch?v=T6m0hnHvZbU&feature=youtu.be.

2.1.3.2. Prospective sources

A single clinical system and a number of experimental proton systems represent prospective sources that will be described in the next section. Most of these systems generate proton beams that are currently too small in size (~100 μm to 1 cm) to be considered for ultrahigh dose-rate irradiations outside of *in vitro* and *in vivo* experiments.

Firstly, the HyperScan proton therapy system (Mevion Medical Systems, Littleton, MA) is based on a superconducting synchrocyclotron directly mounted on a gantry. It operates with proton beam energies up to 230 MeV and a clinical beam current of 6 nA that can be increased to 30 nA for non-clinical purposes. The beam may be delivered with pulse widths of 1–20 μs and PRF of 750 Hz, which results in an intra-pulse dose rate ($\dot{D}_P$) of 13×10^3 Gy s^{-1} and average dose rates of $\overline{\dot{D}} = 200$ Gy s^{-1} at a beam current of 30 nA (Bouchet 2019). The dose rate in the Bragg peak of a passively scattered HyperScan beam has been measured to be $\overline{\dot{D}} = 226$ Gy s^{-1} (Darafsheha *et al* 2020).

The HVE 5.5 MV Singletron accelerator (High Voltage Engineering Europa B.V., Amersfoort, Netherlands) at the Radiological Research Accelerator Facility (RARAF) at Columbia University has been shown capable of delivering protons with $\overline{\dot{D}}$ between 0.025 Gy s^{-1} to 1500 Gy s^{-1} by simply changing the proton beam current accordingly (Buonanno *et al* 2019). Buonanno *et al* used the Singletron to deliver 4.5 MeV protons to human lung cells using a beam spot with a diameter of ~11 mm while achieving dose homogeneity of 3%.

At TRIUMF (Vancouver, Canada), a cyclotron-based proton source is available which hosts a number of beamlines. The main cyclotron accelerates protons to 70–500 MeV with $\overline{\dot{D}}$ up to 17×10^3 Gy s^{-1}, thanks to the capability to deliver with beam currents of up to 100 μA. The TRIUMF proton beamlines can operate with a 1%–95% duty cycle, namely using 10–950 μs pulses delivered at a frequency of 1 kHz. The maximum intra-pulse dose rate ($\dot{D}_P$) of 17×10^3 Gy s^{-1} corresponds to a mean dose rates of $\overline{\dot{D}} = 17 \times 10^3$ Gy s^{-1} and $\overline{\dot{D}} = 170$ Gy s^{-1} for the 950 μs and 10 μs pulse widths, respectively. Deliverable proton pencil beams are ~1 cm in diameter, but beam scanning for irradiation of larger targets is currently not available (Blackmore 2019).

The ion microbeam SNAKE (Superconducting Nanoprobe for Applied nuclear [Kern] physics Experiments) at the 14 MV Munich tandem accelerator represents another high-intensity proton beam source. SNAKE delivers single ~1 ns, 20 MeV proton pulses which are 100×75 μm^2 in size and can accommodate a DPP of up to 5 Gy and PRF of 2.5 MHz (Dollinger *et al* 2009). This source has previously been used for ultrahigh dose-rates irradiations of cancer and normal cells (Auer *et al* 2011, Schmid *et al* 2011). However, for small animal irradiations, a 7 mm diameter target was instead irradiated by means of magnetic, electron and mechanical scanning of a 100×100 μm^2 beam with DPP of ~20 Gy, but this required a total irradiation of 45 min (Zlobinskaya *et al* 2014). The timing of this experiment highlights the limitations of this source in delivering FLASH-RT to small animals.

Particle beams generated by compact laser-driven accelerators are considered a cost-effective alternatives to conventional medical particle accelerators; unfortunately, they currently suffer from unreliable beam generation and transport (Karsch *et al* 2017). Nevertheless, laser-driven TNSA (Target Normal Sheath Acceleration) proton sources have already been employed for ultrahigh dose-rate cell irradiations (Yogo *et al* 2009, 2011, Zeil *et al* 2013, Bayart *et al* 2019) and two such sources are briefly described here. Presently, the main limiter for the use of laser-driven sources is their low PRF, typically a few Hz, which restricts their applicability to high DPP single-pulse irradiations. While current laser-driven proton sources are therefore not capable of delivering tens of Gy in a single pulse, as is nominally required for FLASH-RT, they are discussed here as prospective sources in light of ongoing development.

As a first example of laser-driven proton sources, the ultra-short pulse Ti:Sapphire laser system Draco at the HZDR provides 1.8 J on target which is contained in a pulse of 30 fs duration and a peak intensity of 5×10^{20} W cm^{-2}. The 2×6 mm^2 proton beam generated by the TNSA mechanism, which underpins the acceleration of the laser-driven particle beam, exhibits an exponential energy spectrum with a cut-off at 15 MeV. Using the Draco laser proton accelerator, an ultra-short pulse with DPP of 81 mGy can be delivered so as to achieve dose rates up to $\dot{D}_P = 4.9 \times 10^7$ Gy s^{-1} (Richter *et al* 2011, Zeil *et al* 2013).

The 200 TW SAPHIR (Amplitude Technologies) laser source at the LOA is similarly used as the driver for proton beam acceleration. The SAPHIR laser pulse-duration is 26 fs and the energy on target is 3 J per pulse, resulting in on-target intensities approaching 10^{20} W cm^{-2}. A single proton pulse of 0.7 Gy can be delivered in 4.8 ns to a 2 cm^2 area, which results in $\dot{D}_P = 1.5 \times 10^8$ Gy s^{-1} (Pommarel *et al* 2017). Table 4 summarizes the discussed FLASH proton sources.

Table 4. Summary of ultrahigh dose-rate proton sources and their selected operating parameters.

	Manufacturer	Max. E (MeV)	Max. current (μA)	Max. $\overline{\dot{D}}$ (Gy s^{-1})	Ref.
Proteus	IBA	230	0.5	200	(Bloch 2019)
HyperScan	Mevion	230	0.03	220	(Bouchet 2019)
ProBeam	Varian	250	0.8	240	(Abel 2019)
TRIUMF	Experimental	500	100	17×10^3	(Blackmore 2019)
SNAKE	Experimental	20	0.08	12.5×10^6	(Dollinger *et al* 2009)

Table 5. A summary of a selected ultrahigh dose-rate sources with their mean $\overline{\dot{D}}$ and instantaneous $\dot{D}_P$ dose rates.

				Dose rate (Gy s^{-1})	
Radiation	Type	Source	Energy	$\overline{\dot{D}}$	$\dot{D}_P$
Protons	Medical	HyperScan	230 MeV	200	13×10^3
X-rays	Synchrotron	ESRF	102 keV[a]	37	18×10^3
Electrons	Non-medical	Kinetron	4.5 MeV	1000	2×10^7
Electrons	Medical	Clinac EX	9 MeV	900	1.7×10^6
VHEE	Experimental	NLCTA	120 MeV	90	9×10^{12}

[a]Maximum intensity.

2.1.4. Beam microstructure

FLASH radiation delivery to date has mainly been achieved with linac-, synchrotron-, and cyclotron-based sources that each are characterized with a different beam time structure. Some studies suggest that the FLASH effect is observed only for pulsed beams delivering a high intra-pulse (instantaneous) dose rate $\dot{D}_P$. The beam microstructure is therefore deemed to be an important parameter for the FLASH effect. Table 5 summarizes the mean $\overline{\dot{D}}$ and intra-pulse $\dot{D}_P$ dose rates for a selection of representative ultrahigh dose-rate sources that were presented in sections 2.1.1–2.1.3. It can be noted that the highest $\dot{D}_P$ of 9×10^{12} Gy s^{-1} can be achieved for an experimental VHEE source at the NLCTA which might remain compatible for use in ultrahigh dose-rate experiments considering the mean dose rate $\overline{\dot{D}} = 90$ Gy s^{-1}. Similar sources could be used for future *in vivo* studies in order to investigate a wide parameter space related to the beam microstructure.

The outcomes of FLASH-RT, which include a marked improvement in normal tissue sparing (see section 3), have often been compared to conventional irradiations performed with sources delivering continuous radiation, such as with a ^{137}Cs-137 source or the ~220 kV x-ray source found on small-animal image guided irradiators. The use of continuous, rather than pulsed, radiation could possibly affect the biological damage response in both cancerous and healthy tissues. Interestingly, in a recent study it was demonstrated that conventional x-ray tubes could also be capable of delivering continuous beams with dose rates up to 120 Gy s^{-1} at shallow depths in tissue (Bazalova-Carter and Esplen 2019).

Figure 2 summarizes selected presented electron, photon and proton sources in terms of achievable maximum intra-pulse and mean dose rates.

2.2. Dosimetry

2.2.1. Ionization chambers

IC are standard detectors for reference dosimetry in clinical RT settings and are highly valuable for their ability to provide real-time dose measurements. ICs calibrations are traceable to national standards/metrology laboratories, and accurate dose measurements are made possible through the application of recognized dosimetric protocols involving various correction factors (Almond *et al* 1999, Andreo *et al* 2000, Mcewen *et al* 2014) In the context of FLASH-RT, however, the use of non-standard beams and ultrahigh dose-rates disallows the direct application of these standard protocols. Moreover, in order for ICs to be used as reference dosimeters in high $\overline{\dot{D}}$ and DPP fields, the non-negligible effects of ion recombination must be carefully accounted for (Burns and Mcewen 1998, Bruggmoser *et al* 2008, Kry *et al* 2012, Karsch 2016, Petersson *et al* 2017).

In general, ICs suffer from reduced ion collection efficiency within intense radiation fields and thus require the calculation of an associated correction factor (k_s in IAEA 398 convention). For low LET radiations commonly employed by clinical accelerators, these saturation effects are due primarily to volume recombination, which is known to be dependent on the DPP, chamber construction (i.e. electrode spacing) and polarization voltage (Boag 1966, Derikum and Roos 1993, Bruggmoser *et al* 2008, Karsch 2016). For pulsed clinical accelerators under conventional operation with DPP < 1 mGy, the corrections are generally modest and <5% (Almond *et al* 1999, Kry *et al* 2012), but have been found to increase substantially in

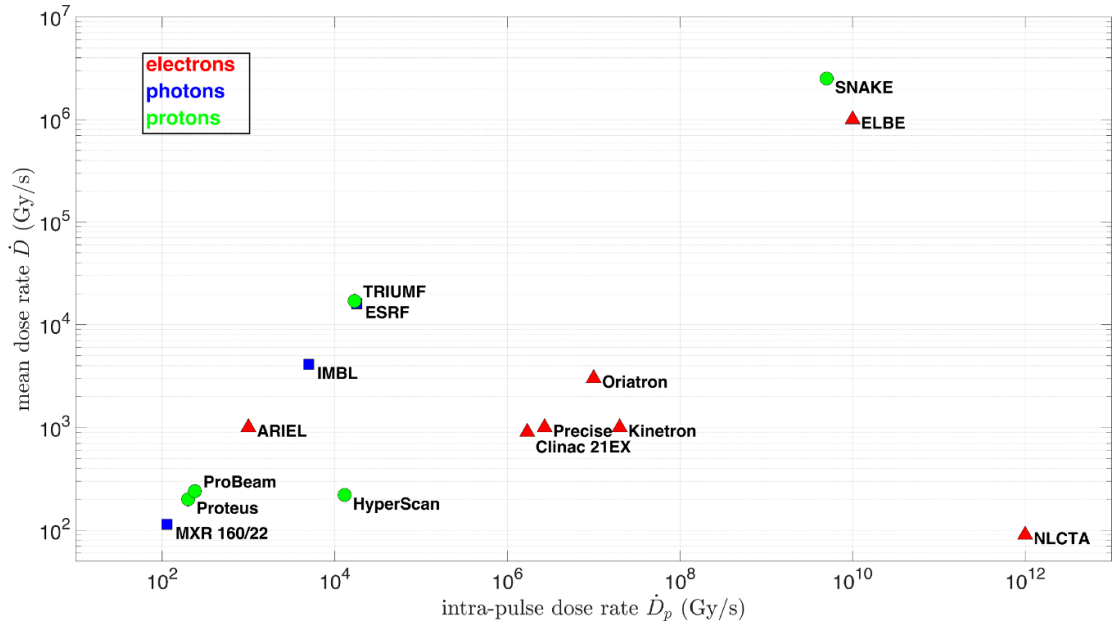

Figure 2. Intra-pulse and mean dose rates for selected ultrahigh dose-rate sources.

very-high DPP beams such as those relevant to FLASH-RT (Petersson *et al* 2017, Jorge *et al* 2019). For continuous sources, similar corrections are necessary but may be treated according to slightly different theoretical models (Boag and Wilson 1952, Palmans *et al* 2006, Karsch 2016, Liszka *et al* 2018).

High DPP irradiations, which require non-negligible corrections for saturation effects, have become increasingly commonplace: FFF, intraoperative radiotherapy, active scanning proton and other emerging laser accelerated particle sources, for example, are concerned with DPP values well above those used in routine clinical RT (i.e. >1 mGy). As such, there has been a growing demand to determine the requisite recombination corrections over a wider range of DPP values (i.e. few mGy to cGy), applicable to the various modalities (Di Martino *et al* 2005, Laitano *et al* 2006, Bruggmoser *et al* 2008, Sutton and Littler 2017, Gotz *et al* 2017). However, in the context of treatments that would employ ultrahigh dose-rate/DPP irradiations, the reduction in collection efficiency becomes increasingly severe and so correction factors along with the underlying methodologies must be carefully evaluated before ICs might be reliably utilized for reference dosimetry at ultrahigh dose-rates. Unfortunately, existing recombination models and calculation procedures, namely those concerned with pulsed beams, have been limited in their ability to determine these corrections at DPP values of 10 Gy suitable to FLASH-RT (Gotz *et al* 2017, Petersson *et al* 2017).

Efforts have been made to establish the range of DPP values for which various existing (Boag *et al* 1996, Burns and Mcewen 1998) or newer recombination models (Karsch 2016, Gotz *et al* 2017) can be applied to quantify the effects of ion recombination on IC responses in high DPP (Piermattei *et al* 2000, Cella *et al* 2010, Wang *et al* 2012, Ghorbanpour Besheli *et al* 2016) and, more recently, ultrahigh dose-rate contexts (Petersson *et al* 2017, Gotz *et al* 2017, Liszka *et al* 2018). A number of the relevant ICs are here introduced and pertinent details of the ion recombination correction factor (k_s), as well as chamber models suitable for application in high DPP/dose-rate (pulsed and continuous) fields, are elaborated upon.

2.2.1.1. Chamber models

chambers have been well described for use in high $>10^{-2}$ Gy *DPP* settings and with accepted protocols, such as those intended for use in FFF (Kry *et al* 2012, Wang *et al* 2012, Sutton and Littler 2017) and IORT (Piermattei *et al* 2000, Di Martino *et al* 2005, Bruggmoser *et al* 2008, Cella *et al* 2010, Ghorbanpour Besheli *et al* 2016) applications. More recently, a number of chambers along with appropriate saturation corrections have been evaluated for use in ultrahigh dose-rate beams for photons (Prezado *et al* 2011b, Crosbie *et al* 2015, Fournier *et al* 2016), electrons (Petersson *et al* 2016, 2017), and protons (Liszka *et al* 2018, Patriarca *et al* 2018). The corresponding modalities of interest range from synchrotron spatially-fractionated and broad-beam (Bräuer-Krisch *et al* 2015, Smyth *et al* 2018), laser-accelerated particles (Karsch *et al* 2011, Richter *et al* 2011, Zeil *et al* 2013) and, more recently, and FLASH-RT using photons (Montay-Gruel *et al* 2018), electrons (Petersson *et al* 2016, Montay-Gruel *et al* 2017, Jorge *et al* 2019, Bourhis *et al* 2019b) and protons (Beyreuther *et al* 2019a).

To date, plane-parallel chambers have been investigated for use at higher DPP $= 10^{-2}$–10^{-1} Gy electron beams for IORT, based on application of the existing formalisms and variants thereof (Piermattei *et al* 2000, Di Martino *et al* 2005, Laitano *et al* 2006) for standard chambers including the Markus (23343) and Roos (34001) chambers (PTW Freiburg, Freiburg, Germany), the Wellhofer chamber (Scanditronix, Schwarzenbruck, Germany) and the NACP-02 chamber (IBA Dosimetry, Schwarzenbruck, Germany). Bruggmoser *et al* (2008) demonstrated, for example, the applicability PTW Roos (34001) and Farmer-type (30013) chambers for DPP as high as 41 mGy.

It is important to note that the DPP and the intra-pulse dose rate can affect the overall treatment time, which may be a critical parameter for the initiation of the FLASH effect (Bourhis *et al* 2019a). Unfortunately, the DPP ranges for which many well-established chamber and saturation model combinations exist are not compatible with the very high-DPP pulsed beams that have been employed in FLASH-RT. Therefore, to enable IC dosimetry in these contexts, special attention should be directed to those chambers which have been characterized for ultrahigh dose-rate irradiations and bearing saturation corrections which do not preclude accurate dose measurements under such conditions.

The suitability of the commonly used Roos and Farmer chambers to conditions encountered in FLASH-RT has not been shown. It may be inferred from past studies investigating k_s in FFF and IORT domains, where large saturation corrections already become apparent, that they are quite poorly suited for use in high dose-rate fields. In contrast to these conventional chambers, small-volume ICs have often been employed in non-standard fields, both with respect to field size (i.e. stereotactic and small-animal RT) and dose-rate (FFF, IORT). For routine deliveries for which standard dosimetry protocols (i.e. TRS 398, TG-51) are suitable, very small <0.05 cm^3 chambers are not recommended for reference dosimetry, typically due to anomalous recombination behavior (i.e. increased charge multiplication effects), asymmetric and field-size dependent polarity effects (Agostinelli *et al* 2008, Looe *et al* 2018) or high-Z chamber electrodes (Mcewen *et al* 2014). However, it has been demonstrated that such ICs feature lower k_s correction factors compared to their large-volume counterparts both experimentally (Wang *et al* 2012, Sutton and Littler 2017) and theoretically (Gotz *et al* 2017). This is in agreement with the standard theory of recombination (Boag and Wilson 1952, Boag 1966, Boag and Currant 1980, Boag *et al* 1996), in which the degree of ion recombination is proportional to the electrode distance and electric field strength within the chamber (Gotz *et al* 2017). Thus, it stands to reason that small-volume ICs, featuring smaller electrode gaps (or effective spacing in the case of cylindrical chambers) may be more appropriate to conditions of high dose-rate or high DPP dosimetry.

ICs best suited for use in ultrahigh dose-rate dosimetry should suffer as little from saturation effects as possible in order to minimize the magnitude of the associated correction factor and the uncertainty introduced by its calculation (Petersson *et al* 2017). Consequently, the trend of using small-volume ICs has been extended to ultrahigh dose-rate modalities. The Advanced Markus IC (PTW-34045), for example, has found use in the dosimetric evaluation the Oriatron RT6 currently in use for FLASH irradiations at Lausanne University Hospital (Petersson *et al* 2016, Montay-Gruel *et al* 2017, 2019, Jaccard *et al* 2018, Jorge *et al* 2019). The chamber was well-characterized in the work of Petersson *et al* (Petersson *et al* 2017) and it was determined that, through careful determination of appropriate recombination k_s and polarity k_p corrections factors, the dose uncertainty using a chamber-specific semi-empirical model for recombination could be reduced to 2.8%. The authors developed models, specific to their irradiation setup, which spanned a wide range of DPP values (0.3 mGy to 10 Gy) and demonstrated that the ion recombination effects were largely independent of the mean ($\bar{\dot{D}}$) or intra-pulse ($\dot{D}_P$) dose-rates, up to 1.3×10^3 and 7×10^6 Gy s^{-1}, respectively, so long as the *DPP* remained constant.

The PTW PinPoint (31014) and Semiflex (31010) chambers have found frequent use in ultrahigh dose-rate (kGy s^{-1}) synchrotron therapies where a continuous (PRF of MHz) x-ray source is used to deliver 10^2–10^3 Gy doses over short <1 s time scales in order to maintain compatibility with micro- and mini-beam therapies, in which avoidance of intrafraction motion is paramount. Importantly, both the source and the ICs utilized are theoretically compatible with the mean dose-rates that may be encountered (~10^2 Gy s^{-1}) during FLASH-RT. Notable synchrotron photon FLASH experiments have been completed (Montay-Gruel *et al* 2018, Smyth *et al* 2018) with active dosimetry provided by the PTW PinPoint chamber and protocols adapted from international recommendations (Fournier *et al* 2016, Lye *et al* 2016). In the study of Montay-Gruel *et al* (2018), the PinPoint IC was used to measure the dose-rate prior to the biologic dose delivery. The PinPoint chamber has been recommended (Fournier *et al* 2016, Livingstone *et al* 2017) over the Semiflex model used in earlier synchrotron protocols (Prezado *et al* 2011b), in large part due to the reduced volume and saturation effects, although both chambers are still applied as reference dosimeters within high dose-rate settings for detector cross-calibration (Livingstone *et al* 2016a).

For proton therapy modalities, where beams are often treated as continuous insofar as recombination effects are concerned, the correction factors tend to be much lower (<1%) even in high 10^1–10^2 Gy s^{-1} dose-rate contexts (Gomà *et al* 2014, Patriarca *et al* 2018). Chambers used under these conditions include the plane-parallel Markus (PTW-23343) and above-mentioned Advanced Markus (PTW-34045) (Liszka *et al* 2018, Beyreuther *et al* 2019a). However, Patriarca *et al* (2018) used the CC01 chamber (IBA Dosimetry, Schwarzenbruck, Germany), which was calibrated for their 198 MeV (pristine Bragg peak) beam, and found to be consistent (<5%) with EBT-3 Gafchromic films for $\bar{\dot{D}}$ between 0.05–40 Gy s^{-1}. The ion recombination was less than 1% in this dose-rate range and the dose response between 0.25–20 Gy dose was linear to within 1.5%.

A selection of ICs which have been utilized directly in ultrahigh dose-rate applications are summarized in table 6 along with physical parameters of general interest.

2.2.1.2. Models for ion recombination correction factors

In accordance with current dosimetry protocols, ion recombination correction factors (k_s) must be determined by application of theoretical models or experimental measurement. This is traditionally done by either multi-voltage analysis and extrapolation of Jaffe plots (Jaffé 1913) or more routinely by two-voltage analysis (TVA) (Boag and Currant 1980, Weinhous and Meli 1984), as recommended in current clinical protocols (i.e. IAEA TRS-398 and AAPM TG-51), so long as the chamber is operated at a polarizing voltage where linearity of the IC response is maintained. In fact, it is recommended that the range of polarizing voltages and DPP values for which linearity maintained is first characterized before using an IC for reference dosimetry (Bruggmoser *et al* 2008, Mcewen *et al* 2014, Liszka *et al* 2018). The appropriate choice of formalism ultimately depends on the beam microstructure, and whether it can be considered as continuous or pulsed insofar as the underlying theory is concerned.

The pulsed formalism for recombination based on Boag theory (Boag and Wilson 1952, Boag *et al* 1996) requires that the pulse width (t_b) is shorter than the ion collection time (t_c) of the IC (i.e. $t_b < t_c$), which in turn must be shorter than the inverse PRF (i.e. $(1/PRF) > t_c$). For high PRF pulsed-scanned or quasi-continuous beams (i.e. $t_b > t_c$), however, a continuous formalism must instead be used, such as the TVA formulation applicable to continuous beams (IAEA TRS 398) (Boag and Wilson 1952, Andreo *et al* 2000). Semi-empirical models (Zankowski and Podgorsak 1998, Bruggmoser *et al* 2008), recently applied for example by Petersson *et al* Petersson *et al* (2017) and Aldosary *et al* (Aldosary *et al* 2017), and new theoretical formalisms for beams of arbitrary PRF (Karsch 2016) or with high DPP (Gotz *et al* 2017), have been devised which may better account for the extreme recombination effects observed during IC dosimetry of ultrahigh dose-rate beams. These new correction techniques are particularly important for high DPP beams delivered by existing FLASH-capable (i.e. Oriatron, Kinetron) (Petersson *et al* 2017) and forthcoming VHEE (i.e. laser plasma) accelerator technologies (Gotz *et al* 2017). Moreover, for synchrocyclotron proton beams capable of ultrahigh dose-rate delivery (i.e. IBA S2C2), a three-voltage method may be employed that can also be extended to higher-LET (i.e. light-ion) beams where initial recombination effects become non-negligible and may prohibit the use of conventional TVA methods (Rossomme *et al* 2020). Ultimately, a critical consideration before calculation of k_s is whether a pulsed beam, for a given selection of IC, should be treated as continuous or not. In the case of pulsed radiation beams, the degree of ion recombination will depend on the DPP rather than the mean or intra-pulse dose-rates of the beam (Bruggmoser *et al* 2008, Petersson *et al* 2017).

2.2.2. Radiochromic films

Radiochromic films are self-developing radiation dosimeters whose detection principle relies on radiation-induced polymerization of an active (diacetylene) layer resulting in coloration and a measurable increase in optical density (OD) (Rink *et al* 2008, Kouloukidis *et al* 2013). The most common radiochromic films, Gafchromic films, are inherently 2D and have been consistently demonstrated as having low dose-rate and energy dependencies, as discussed herein. These features are standout as being desirable for application in a ultrahigh dose-rate dosimetry to provide absolute dose, dose-rate and dose distribution data in the highly variable, non-standard beams utilized in the current FLASH-RT landscape.

To date, Gafchromic films of various generations have been successfully utilized as convenient systems for dose measurement for both routine and non-standard fields (Niroomand-Rad *et al* 1998, Wilcox and Daskalov 2007, Chung *et al* 2010, Devic 2011, Borca *et al* 2013, Palmer *et al* 2015). EBT type films have been employed as reference dosimeters for stereotactic applications, where superior detector resolution is required owing to steep dose gradients of interest (Chung *et al* 2010, Massillon-JL *et al* 2013, Gonzalez-Lopez *et al* 2015). Applications have also extended to high-dose rate modalities, which include VHEE irradiation (Bazalova-Carter *et al* 2015a) and spatially micro-fractionated synchrotron therapies, most notably MRT/MBRT (Crosbie *et al* 2008, Bräuer-Krisch *et al* 2009, Bartzsch and Tag 2014). The high resolution

Table 6. Summary of ICs which have been employed in ultrahigh dose-rate applications along with relevant physical beam and chamber parameters of interest. Data for pulsed (P) or continuous (C) proton (*p*), electron (*e*) and photon (γ) beams are listed.

Chamber	Sensitive volume (cc)[a]	Ion collection time (μs)[a]	Beam type	*DPP* (pulsed) or $\bar{\dot{D}}$ (continuous)[b]	Ref.
Markus (PTW 23343)	0.057	90	*p* (C)	13.4 Gy s^{-1}	(Liszka *et al* 2018)
			e (P)	100 Gy	(Petersson *et al* 2016)
Advanced Markus (PTW 34045)	0.02	22	*e* (P)	10 Gy	(Montay-Gruel *et al* 2017)
			e (P)	~4 Gy	(Jorge *et al* 2019)
			p (C)	100 Gy s^{-1}	(Beyreuther *et al* 2019a)
				16 000 Gy s^{-1}	(Bräuer-Krisch *et al* 2015)
				14 000 Gy s^{-1}	(Crosbie *et al* 2015)
Pinpoint (PTW 31014)	0.015	20	γ (C)	12 000 Gy s^{-1}	(Montay-Gruel *et al* 2018)
				300 Gy s^{-1}	(Lye *et al* 2016)
				4400 Gy s^{-1}	(Archer *et al* 2019)
IBA CC01	0.01	N/A	*p* (C)	~40 Gy s^{-1}	(Patriarca *et al* 2018)
Semiflex (PTW 31010)	0.125	100	γ (C)	~13 000 Gy s^{-1}	(Prezado *et al* 2011a)

[a]Sensitive volume and ion collection time quantities were acquired from vendor websites and direct correspondence. (www.ptwdosimetry.com/en/, www.iba-dosimetry.com/).

[b]Depending on the k_s formalism used, either the (mean) dose-rate or dose-per-pulse (*DPP*) is presented as the relevant quantity for volume recombination in continuous or pulsed beams, respectively.

provided is also relevant for radiobiological small-animal irradiations, which are of immediate relevance to the research aimed toward clinical translation of FLASH-RT.

The dose-rate independence of Gafchromic film has been demonstrated across a number of generations, models and for various modalities and energies, from the precursor to EBT type films was shown to be dose-rate independent from $\overline{\dot{D}} = 0.8$ Gy s^{-1} to 5×10^8 Gy s^{-1} for MeV photons and electrons (Li *et al* 2000). Karsch *et al* (2012) demonstrated that EBT-1 films were dose-rate independent up to $\dot{D}_P = 1.5 \times 10^{10}$ Gy s^{-1} for a 20 MeV pulsed electron beam. The following generation of EBT-2 similarly demonstrated negligible dose-rate dependence for high energy photons, most notably for VHEE applications as demonstrated by Bazalova *et al* (2015a) using a 60 MeV electron beam with $\dot{D}_P$ between 3×10^{12} and 9×10^{12} Gy s^{-1}.

The legacy of dose-rate independence set by these past generations is succeeded by the newer EBT-3 and EBT-XD models; these new varieties consist of a 28 μm and 25 μm thick active layers, respectively, and two symmetric 125 μm thick polyester layers. EBT-3 films have demonstrated dose-rate linearity in ultrahigh dose-rate electron irradiations at $\dot{D}_P$ of up to 8×10^6 Gy s^{-1} for a beam energy between 4.9–6 MeV, depending on dose-rate, and over a wide dose range of 2 Gy to 20 Gy (Jaccard *et al* 2017). Jorge *et al* (2019) cross-verified the dose-rate independence of both EBT-3 and XD films for pulsed electrons delivered at $\overline{\dot{D}} = 1050$ Gy s^{-1} and $\dot{D}_P \sim 1.7 \times 10^6$ Gy s^{-1}, respectively (i.e. 15 Gy in four pulses, 200 Hz, *DPP* of ~3.75 Gy, 2.2 μs pulse width). Lansonneur *et al* (2019) was able to validate their Monte Carlo model of the Kinetron electron linac using against measurement with EBT-XD films for D_p on the order of 10^6 Gy s^{-1}.

EBT films have been validated for use in MRT synchrotron contexts, where kGy s^{-1} dose-rates are routinely encountered (Crosbie *et al* 2008, Bräuer-Krisch *et al* 2009, Bartzsch and Tag 2014), VHEE irradiations (Subiel *et al* 2014, Bazalova-Carter *et al* 2015a), and recently in ultrahigh dose-rate proton irradiations (Patriarca *et al* 2018, Buonanno *et al* 2019, Beyreuther *et al* 2019a). For example, Patriarca *et al* (2018) verified the dose-rate independence of EBT-3 films for 230 MeV protons delivered by a clinical cyclotron at dose-rates up to ~40 Gy s^{-1}, but noticed differences in response between pristine (198 MeV) and (138 MeV) SOBP. Special consideration (due to quenching effects) must be given for protons and heavy ions particularly in regions of highly variable LET, such as within the SOBP (Martišíková *et al* 2008, Kirby *et al* 2010, Fiorini *et al* 2014, Castriconi *et al* 2017).

EBT films are valuable for use in not only electron FLASH, but across various particle modalities. Within the recent literature, for example, EBT-2,3 and XD films have used as passive dosimetry systems for *in vivo* dose measurements in electron FLASH beams delivered using both experimental (i.e. Oriatron eRT6) and modified medical accelerators (Jorge *et al* 2019, Simmons *et al* 2019, Vozenin *et al* 2019a). For synchrotron-generated photons, Montay-Gruel *et al* (2018) used EBT-3 films for dose measurement with $\dot{D}_P$ of approximately 12 000 Gy s^{-1}. In ultrahigh dose-rate proton contexts, Beyreuther *et al* (2019b) employed EBT-3 films for *in vivo* measurements in a 224 MeV proton beam at $\overline{\dot{D}} = 100$ Gy s^{-1} and $\dot{D}_P = 0.5 \times 10^3$ Gy s^{-1}. Buonanno *et al* (2019) used low energy (4.5 MeV) protons from a 5.5 MV singletron (High Voltage Engineering Europa B. V., Amersfoort, the Netherlands) accelerator to irradiate unlaminated EBT-3 films with $D_p = 1000$ Gy s^{-1} (Grilj and Brenner 2018).

Considering this cross-modality relevance of FLASH-RT and its demonstration over a range of particle energies, from kilovoltage photons, low-energy electrons and VHEEs, high-energy protons, a demonstrable energy and particle-type independence are highly desirable traits amongst candidate dosimeters for ultrahigh dose-rate irradiations. For megavoltage radiation, EBT type films across generations have consistently demonstrated these traits and, in addition, the weak energy dependence exhibited in earlier models has improved substantially in recent generations (EBT-3, EBT-XD) (Arjomandy *et al* 2010, 2012, Brown *et al* 2012). The EBT-3 film energy dependence for <100 keV photons has significantly reduced compared to previous models. A lower dependence still was recently observed for EBT-XD films compared to EBT-3, although the overall response remained comparable (to within 3.5%) for energies <100 keV and doses up to 15 Gy (Khachonkham *et al* 2018). The difference in response of EBT-3 for electron energies between 6 MeV and 16 MeV was found to be within 0.5% for a single dose level of 2 Gy (Sipilä *et al* 2016). Recently, the energy independence was explicitly established by Jaccard *et al* (2017), who considered electron energies of 4–12 MeV and doses between 0.25 Gy and 30 Gy, relevant to the large single fractions of FLASH-RT, and were able to demonstrate no appreciable energy dependence.

While the low energy dependence of EBT-3 and EBT-XD films (Reinhardt *et al* 2012, Sorriaux *et al* 2013, Grams *et al* 2015, Miura *et al* 2016, Khachonkham *et al* 2018) as well as previously discussed dose-rate independence both provide significant flexibility while using film dosimetry for FLASH-RT, there remain important LET and energy-related considerations. For example, in EBT-3 films there exist dose-dependent differences in sensitivity to <100 keV x-ray beams, especially for doses below 1 Gy (Massillon-JL *et al* 2013, Eduardo Villarreal-Barajas and Khan 2014, Guerda Massillon *et al* 2016). Consequently, where low-energy (kV) beams are concerned, such as in the context of FLASH-RT delivered with synchrotrons

(Montay-Gruel *et al* 2018) or using modified conventional kV x-ray sources (Bazalova-Carter and Esplen 2019), extra care should be given. Furthermore, LET dependencies can complicate the straightforward application of film dosimetry to particle (proton or ion) beams in which the LET also changes with depth, making characterization of dose at a well-defined measurement point an important consideration.

FLASH-RT is currently characterized by the delivery of high-dose single fractions and therefore the limited sensitivity ranges of EBT films becomes a noteworthy consideration. The dynamic dose range for ETB-3 is 0.1–20 Gy, although suitability up to 40 Gy has also been suggested (Borca *et al* 2013, Chen *et al* 2016). The new EBT-XD film, on the other hand, was recently considered for electron FLASH-RT (Jorge *et al* 2019, Lansonneur *et al* 2019), and features improved sensitivity over EBT-3 for doses >5 Gy (Khachonkham *et al* 2018). Alternatively, one of HD-V2 (replaced HD-810) or MD-V3 (replaced MD-V2-55) can be optimally used within dose ranges of 10–1000 Gy and 1–100 Gy, respectively, but their dose-rate independence and MV energy response have not yet been verified under ultrahigh dose-rate conditions. The HD-V2 film and previous MD and HD type generations have, however, been investigated for use in ultrahigh dose-rate synchrotron x-ray applications (Nariyama 2005, Crosbie *et al* 2008, Martínez-Rovira *et al* 2012) whereby different sensitivities and energy dependence have been identified relative to EBT models. The HD-810 and MD-V2-55 models under-respond, not unlike EBT-3 films, by as much as 50% to photon energies between 30–100 keV, while the newer HD-V2 model over-responds in that same domain (Cheung *et al* 2004, Nariyama 2005, Bartzsch and Tag 2014). The use of these extended-range films should follow careful response characterization for a given beam configuration if they are to be considered for dosimetry in FLASH-RT.

2.2.3. Semiconductor detectors

Semiconductor detectors, here referring to diode, MOSFET and diamond dosimeters, have been previously investigated for use in high intensity radiation fields for applications in MRT/MBRT (Bräuer-Krisch *et al* 2015) and dosimetry of high $\dot{D}_P$ and DPP laser-accelerated electron beams (Karsch *et al* 2017).

2.2.3.1. Silicon diodes and MOSFETS

In the case of conventional semiconductor silicon (Si) diodes, exposure to ultrahigh dose-rate fields will result in enough generated charge to saturate the readout system. To circumvent this critical limitation, new p-type silicon strip detectors (SSD) have been developed to allow reduced saturation through the application of thin <10 μm single-strip sensors (Rosenfeld 2006) and low-resistivity doped substrates to improve the stability and response linearity of the detector (Lerch *et al* 2011, Bräuer-Krisch *et al* 2015, Davis *et al* 2018). The so-called X-Tream dosimetry system, which is based on this SSD technology, can facilitate high spatial-resolution, real-time dose monitoring and has been recently tested at the IMBL for dose-rates >100 Gy s^{-1} (Petasecca *et al* 2012, Fournier *et al* 2017, Davis *et al* 2018).

A commercially-available diode and candidate for ultrahigh dose-rate dosimetry is the PIN-type EDP 20-3G Diode (IBA Dosimetry GmbH, Schwarzenbruck, Germany) and it was used by Lempart *et al* (2019) to measure the output of their modified Elekta linac. The authors were able to demonstrate that the diode response was linear with increasing DPP up to 0.18 Gy ($\overline{\dot{D}} \approx 36$ Gy s^{-1} or $\dot{D}_P \approx 6 \times 10^4$ Gy s^{-1} assuming 3 μs pulse width) with no indication of the saturation trend, which was otherwise observed in the transmission IC of their linac.

MOSFETs have been investigated for use as online, high-spatial-resolution dosimeters for ultrahigh dose-rate kV x-ray beam applications, most notably in synchrotron MRT/MBRT (Rosenfeld *et al* 1999, 2001, Bräuer-Krisch *et al* 2003, Siegbahn *et al* 2009). In contrast to Si diodes, MOSFETs have been used to measure kGy s^{-1} dose-rates, but are not immune to recombination effects and experience saturation over time and thus require replacement after ~1000 Gy of accumulated dose (Siegbahn *et al* 2009). So-called edge-on MOSFET dosimetry offers unparalleled spatial-resolution through direct use of the <1 μm active (edge) element (Lerch *et al* 2011). Therefore, while periodic detector replacement limits the routine practicality of MOSFETs, it may not preclude their usefulness in applications demanding high spatial-resolution. For electron beams, on the other hand, significant temperature increases may cause stability and sensitivity changes following high DPP irradiations that may be intolerable (Favaudon *et al* 2019). Another novel application of semiconductor technology was demonstrated by Reinhardt *et al*, who adopted the RadEye1 commercial photodiode array (Rad-Icon Imaging Corporation, Santa Clara, CA) of dosimetry in a laser-accelerated ns-pulsed proton beam of energies up to 20 MeV (Reinhardt *et al* 2013). The detector was found to be dose-rate as well as particle-type independent, but exhibited an exponential increase in leakage current with accumulated dose. After a radiation dose of about 100 Gy the dynamic range decreased by a factor of 2, which would necessitate frequent detector replacement.

While valued for their online measurement capabilities and small active volumes, Si diode and MOSFET detectors experience significant saturation effects and are non-tissue-equivalent, which necessarily fosters an

energy-dependent response (Siegbahn *et al* 2009, Lerch *et al* 2011, Bräuer-Krisch *et al* 2015). Longevity of operation due to radiation damage may also be concern due to changes in charge carrier density in the surface oxide (MOSFET) or bulk damage to the silicon (diodes) layers whereby dark current increase based on the total deposited dose and is independent on particle type (Reinhardt *et al* 2013, Bräuer-Krisch *et al* 2015). As these detectors continue to improve, the high spatial resolution and small-field dosimetric capabilities of modern semiconductor technologies, along with advancements in the underlying fabrication, may make them attractive for future online dosimetry in FLASH-RT beams.

2.2.3.2. Diamond detectors

Compared to the above silicon-based technologies, diamond detectors present a highly promising alternative in the domain of real-time x-ray dosimetry (Livingstone *et al* 2016b). They are well suited for dosimetry in non-standard field conditions (Ciancaglioni *et al* 2012, Chalkley and Heyes 2014, Morales *et al* 2014, Muir and Mcewen 2015), or higher DPP applications (Di Venanzio *et al* 2015). Moreover, their use in high intensity fields suited to FLASH-RT has been previously investigated (Karsch *et al* 2012, Livingstone *et al* 2016a, 2016b, Patriarca *et al* 2018).

Diamond detectors come in two varieties, natural or synthetic, with the latter being based on chemical vapor deposition (CVD). Favorable properties of diamond detectors include an improved soft-tissue equivalence, mechanical and chemical stability, high sensitivity and high radiation resistance (Bucciolini *et al* 2003, Lárraga-Gutiérrez *et al* 2015). CVD detectors, by contrast, boast improved sensitivity Buttar *et al* (2000) and comparatively low cost along with wider availability and reliability of synthetic diamond crystals (Bucciolini *et al* 2005, Almaviva *et al* 2010, Di Venanzio *et al* 2015). With respect to their dosimetric properties, CVD detectors have been reported as having reduced dose-rate, LET and energy dependence relative to natural diamond models (Hoban *et al* 1994, Rustgi and Frye 1995, Sakama *et al* 2005, Lárraga-Gutiérrez *et al* 2015).

The most notable example of a single-crystal CVD type detector is the microDiamond 60019 detector (PTW, Freiburg, Germany), which boasts a sensitive volume of only 0.004 mm^3 as defined by the depletion region extending through the 1 μm thick intrinsic diamond layer. The dose-rate dependence has been investigated across photon (Chalkley and Heyes 2014, Muir and Mcewen 2015, Lárraga-Gutiérrez *et al* 2015, Livingstone *et al* 2016b), electron (Di Venanzio *et al* 2015) and proton modalities (Marsolat *et al* 2016, Gomà *et al* 2016, Patriarca *et al* 2018). In particular, Gomà *et al* (2016) showed a negligible dose rate dependence of their detector in a scanned 150 MeV proton beam up to 3 Gy s^{-1} and no LET dependence. Patriarca *et al* (2018) recently extended this range for protons up to 40 Gy s^{-1} and found no significant (<5%) dose rate dependence. Response stability and dose linearity have also been consistently reported (Ciancaglioni *et al* 2012, Di Venanzio *et al* 2015, Lárraga-Gutiérrez *et al* 2015, Gomà *et al* 2016) although inter-detector variability has been observed (Marsolat *et al* 2016). While Marsolat *et al* (2016) found the microDiamond detector to be dose-rate independent (up to $\bar{\dot{D}} = 5.52$ Gy s^{-1}) in a 138 MeV passively scattered proton beam, only 50% (2/4) of the identical detectors they tested demonstrated the expected dosimetric properties, including LET and dose-rate independence.

More recently, Livingstone *et al* (2016b) considered the use of microDiamond detectors in ultrahigh dose-rate environments, as applied to synchrotron SFRT. Specifically, the authors were able to demonstrate that no dose-rate dependence between up to $\bar{\dot{D}} = 700$ Gy s^{-1} in the quasi-continuous 95 keV synchrotron beam of the IMBL at the Australian Synchrotron. A very low (<2%) energy dependence above 100 keV was also demonstrated under these intense conditions, in agreement with the manufacturer's claims and previous MV photon beams results (Pimpinella *et al* 2012, Lárraga-Gutiérrez *et al* 2015). Below 100 keV, however, the correction for beam quality becomes non-negligible. Pimpinella *et al* (2012) calculated that for energies between 70 keV and 100 keV, the energy response varies by up to 10%, increasing to 15% below 60 keV. Consequently, kilovoltage beam applications require careful consideration due to under-response at low energy but the response can be quantified and accounted for. Measurements with the microDiamond have been found to agree with those of dose-rate independent Gafchromic EBT-3 films (for $\bar{\dot{D}} = 1$–700 Gy s^{-1}) while simultaneously offering reduced noise and the benefit of real-time dose measurement (Livingstone *et al* 2016b).

Interestingly, a large dose-rate dependence was demonstrated in an earlier study by Karsch *et al* (2012), where the utility of both natural (PTW 60003) and prototype CVD diamond detectors were investigated for use in electron beams with high DPP and intra-pulse (micro-pulse) dose-rates up to $\dot{D}_P = 10^{11}$ Gy s^{-1}. While the saturation of the natural diamond detector was expected (Cirrone *et al* 2003), the dose-rate dependence of the CVD detector has not been reported in the new PTW microDiamond model. It is worth noting, however, that the pulsed time structure of the intense, low-frequency electron beam (ELBE, see sources section 2.1.1.2) used by Karsch *et al* (2012) differs greatly from the synchrotron source at IMBL

utilized by Livingstone *et al* (2016b). Besides the obvious difference in radiation type, the ELBE irradiations in the former study used an electron source with a low 10 Hz *PRF* at low DPP but very-high pulse dose-rates, whereas the effective PRF of the IMBL source was 500 MHz (Dowd *et al* 2008). As a result, the kGy mean dose rate achieved with the IMBL source is a product of the high *PRF* rather than high intra-pulse dose-rate. The suitability of diamond detectors in high-intensity electron beams is nevertheless being brought into question as more recent FLASH irradiations with the Kinetron have also demonstrated a degree of dose-rate non-linearity (Favaudon *et al* 2019).

Altogether, the PTW microDiamond (60019) single-crystal CVD detector stands to be an attractive candidate for application in x-ray and proton FLASH-RT dosimetry and may provide an alternative to ICs or Si-based dosimeters insofar for real-time dosimetry. The relatively consistent dose-rate and energy independence (>100 keV) may relax the need to apply correction factors and thus save on time and complexity during routine dosimetry for FLASH-capable systems. However, care must be given to characterization of each detector due to variability in the stability, sensitivity, as well as LET, energy and dose-rate dependencies across individual detectors of the same model and make (Marsolat *et al* 2016, Livingstone *et al* 2016b).

2.2.4. Plastic scintillating dosimeters

Plastic scintillating dosimeters, in both 2D and fiber-optic varieties may be useful for ultrhigh dose-rate dosimetry considering their apparent utility within high-intensity synchrotron-generated x-ray (Archer *et al* 2019), scanned ion (Russo *et al* 2017)and electron linac (i.e. Kinetron) sources to date (Favaudon *et al* 2019). Of particular relevance, is the Lynx (IBA, Schwarzenbruck, Germany), a commercially available 2D scintillator detector that can provide high-resolution, real-time relative dosimetry for charged particle beams. It consists of a 0.4 mm thick gadolinium-based plastic scintillating screen, coupled to a CCD camera. The screen boasts an active surface area of (300 × 300) mm^2 with an effective spatial resolution of 0.5 mm as well as a variable aperture collimator to allow modification of the amount of light reaching the CCD. The system provides comparable spatial resolution (0.5 mm) when compared to EBT-3 films (~0.2 mm) and has demonstrated good dose linearity, short-term stability as well as a desirable energy and dose-rate independence (Russo *et al* 2017). However, the detector response has also been found to be strongly dependent on radiation LET, which disallows its use in proton depth-dose measurements, for example. To date, the Lynx detector has been used for dose homogeneity measurements within high dose-rate proton (Liszka *et al* 2018, Beyreuther *et al* 2019b), and electron (Lansonneur *et al* 2019) beams. Furthermore, relative dose measurements in a 230 MeV passively scattered proton beam up to 40 Gy s^{-1}, were found to agree with other detectors to within 5% and included a PTW microDiamond detector, the IBA CC01 IC and EBT-3 films (Patriarca *et al* 2018). In ultrahigh dose-rate electron beams, the system has also demonstrated good dose linearity along, reproducibility and stability for dose-rates up to 3.5 × 10^6 Gy s^{-1}, albeit with a relatively narrow dynamic range in the CCD camera (Favaudon *et al* 2019). Although no does measurements have been reported, the response linearity with the pulse width (i.e. DPP) and the grid voltage (i.e. dose-rate) have effectively been demonstrated.

The favorable properties of plastic scintillators for dosimetry in high intensity charged particle or photon beams also extends to fiber-optic plastic scintillating detectors (PSDs). Due to their high spatial-resolution, near water equivalence, radiation hardness and energy independence (Beddar *et al* 1992, Beaulieu and Beddar 2016), these small-field detectors are finding use in ultrahigh dose-rate synchrotron microbeam therapies (Archer *et al* 2019). In high intensity fields, radiation hardness becomes particularly important to avoid detector sensitivity deviations over time, a problem which is encountered in solid-state detectors such as MOSFETs. The application of a PSD within ultrahigh dose-rate synchrotron x-ray fields was demonstrated by Archer *et al* (2019) for dose rates up to ~4000 Gy s^{-1} and a field size of (20 × 20) mm^2. The authors evaluated a PSD comprised of a ~10 μm thick film of BC-400 plastic scintillator optically coupled to a 1 mm diameter optical fibre. One general limitation of PSDs includes so-called stem-effects, which are comprised of Cherenkov radiation and radioluminescence contributions to the total scintillator light signal. For kV synchrotron radiation there is negligible Cherenkov radiation generated and so radioluminescence dominates, notably at lower wavelengths (Therriault-Proulx *et al* 2013); however, for MV photons Cherenkov light would be expected to become an important contributor to the overall stem effect. In the PSD investigated by Archer *et al* (2019), radioluminescence was significant (up to ~52%). Unfortunately, an overlap between the radioluminescence and scintillation spectra limits common methods of correcting for the strong stem effects and ongoing developments are required for efficient corrections if using a second, 'radioluminescence-only', PSD is to be avoided (Archer *et al* 2019).

2.2.5. Alanine dosimeters

Due to their low energy response and wide range of measurable doses, alanine dosimeters have been widely used for high dose dosimetry at national laboratories and for industrial purposes (Sharpe *et al* 1996) and have been used for dose verification of FLASH delivery (Bourhis *et al* 2019b). Doses in the range from 1 to 1×10^5 Gy for 0.1–30 MeV electrons and photon beams can be measured with alanine dosimeters (International Standardization Organization 2004). The dosimeters have shown dose-rate dependence as a function of delivered dose, but this effect was not significant for delivered doses $<5 \times 10^3$ Gy (Desrosiers *et al* 2008). For continuous and pulsed electron beams, alanine dosimeters are dose rate independent up to dose rates of $\bar{\dot{D}} = 10^2$ Gy s^{-1} and $\dot{D}_P = 3 \times 10^{10}$ Gy s^{-1}, respectively (Kudoh *et al* 1997) and may be considered as a suitable dosimeter for FLASH-RT.

2.2.6. Other

Thermoluminescent dosimeters (TLDs) have long been used in conditions of irradiations at ultrahigh dose-rates (Nias *et al* 1970, Epp *et al* 1972, Schulz *et al* 1978), which bears particular relevance to FLASH-RT. They have been previously established as dose-rate independent up to 2×10^8 Gy s^{-1} for pulsed electron beams (Karzmark *et al* 1964, Tochilin 1966) and have been used as reliable, compact replacements for absolute dose measurement in place of costly and labor-intensive chemical dosimeter systems. For example, Tochilin and Goldstein (1966) investigated both CaF and LiF TLDs and demonstrated the dose-rate independence for pulsed MV photon beams up to $D_p \sim 10^9$ Gy s^{-1}. More recently, however, Karsch *et al* (2012) extended the range of independence in electron beams to $\dot{D}_P = 4 \times 10^9$ Gy s^{-1} for LiF-100 TLDs and Jorge *et al* (2019) verified the dose-rate independence against alanine and EBT-3 film passive dosimeters for $\bar{\dot{D}}$ of up to 1050 Gy s^{-1}. TLDs have been used recently by Jaccard *et al* (2017) and Jorge *et al* (2019) with the Oration eRT6 electron accelerator for FLASH treatments and further applied for *in vivo* surface dose measurement in electron FLASH-RT. Their application in ultrahigh dose-rate microbeam therapy applications is also notable through the development of a 2D TLD dosimetry system comprising LiF:Mg,Cu,P (MCP-N)-based TL foils and a reader equipped with a CCD camera capable of <100 μm resolution (Olko *et al* 2006, Ptaszkiewicz *et al* 2008).

Optically-stimulated luminescence dosimeters (OSLDs) bear similarity to TLDs in their mode of operation and functional application. The dose rate dependence for OSLDs may derive from the physical principles of detector response which are similar to those of TLDs (Chen and Leung 2001). Support for the dose independence for OSLDs was provided by Karsch *et al* (2012), who demonstrated no dependence on dose-rate up to approximately $\dot{D}_P = 4.7 \times 10^9$ Gy s^{-1}. For both TLDs and OSLDs, the authors could not rule out the possibility of a dependence on very high DPP values, which were not the subject of investigation. Contrary to this concern, however, high *DPP* settings (up to 10 Gy) have not precluded the reliable use of TLD/OSLDs for reference dosimetry elsewhere in the FLASH literature (Jaccard *et al* 2017, Jorge *et al* 2019).

Chemical dosimeters, such as Fricke dosimeters, have long been established as dose-rate independent reliable media for absolute dosimetry. The downside of such a dosimeter includes high cost, insensitivity to low doses and low spatial-resolution (ICRU 1982, Di Martino *et al* 2005). However, for passive dosimetry on fixed beam lines, for example, their application has been historically routine and generally reliable; with the reliable substitution of dose-rate independent dosimeters (i.e. TLDs, films, alanine), however, its use for measuring dose in radiobiological or clinical contexts has largely diminished.

Methyl viologen radical dosimetry, with a basis in pulse electron radiolysis studies (Favaudon *et al* 1990, Das *et al* 2003), is another dose-rate independent technique which has been employed more recently in ultrahigh dose-rate contexts (Petersson *et al* 2017, Favaudon *et al* 2019). The basis for dose measurement is derived from an optical detection of the blue methyl viologen radical cation (MV+) in N2O-saturated formate buffer where water radiolysis generates OH, H and hydrated e− radicals which are subsequently converted into MV+ (Favaudon *et al* 2019). As an alternative is to other chemical dosimeters operating at sub-microsecond timescales, this dosimetric technique is useful on the basis it can provide in real-time dosimetry at ultrahigh dose-rates (>10^7 Gy s^{-1}), but requires an elaborate and temporally (pulse) synchronous optical system for the requisite transmittance measurements. Moreover, irradiations should be short (<1 s) to avoid the need for measurement corrections due to secondary decay of the MV cation, although such sub-second time scales remain compatible with current FLASH-RT techniques.

Alternative chemical dosimeters, include polymer gels which boast the added benefit of 3D dose readout via CT (McErlean *et al* 2016) or MRI (Maryanski *et al* 1993). Traditional polymer gels are, however, known to be sensitive to dose-rate and also have a limited range of dose applicability (Maryanski *et al* 1993). MRI readout techniques have been implemented for broad-beam synchrotron treatments at lower dose rate (Boudou *et al* 2007). The novel radiochromic gel dosimeter (PRESAGE™), stands as an exception to this case, having demonstrable dose-rate and energy independence, though this has yet to be established at

Table 7. Dosimeters (not including ICs) successfully employed in ultrahigh dose-rate dosimetry. The maximum reported instantaneous dose-rate for which each dosimeter has demonstrated dose-rate independence is included with the corresponding radiation modality.

Dosimeter	$\dot{D}_P$(Gy s^{-1})	Radiation type (γ, e^-, p^+)	Ref.
EBT-3 Film	8×10^6	e−	(Jaccard *et al* 2017)
PTW microdiamond (60019)	700	γ	(Livingstone *et al* 2016b)
LYNX 2D scintillator	3.5×10^6	e−	(Favaudon *et al* 2019)
Alanine	3×10^{10}	e−	(Kudoh *et al* 1997)
TLD-100	4.7×10^9	e−	(Karsch *et al* 2012)
Methyl Viologen	2×10^7	e−	(Favaudon *et al* 2019)

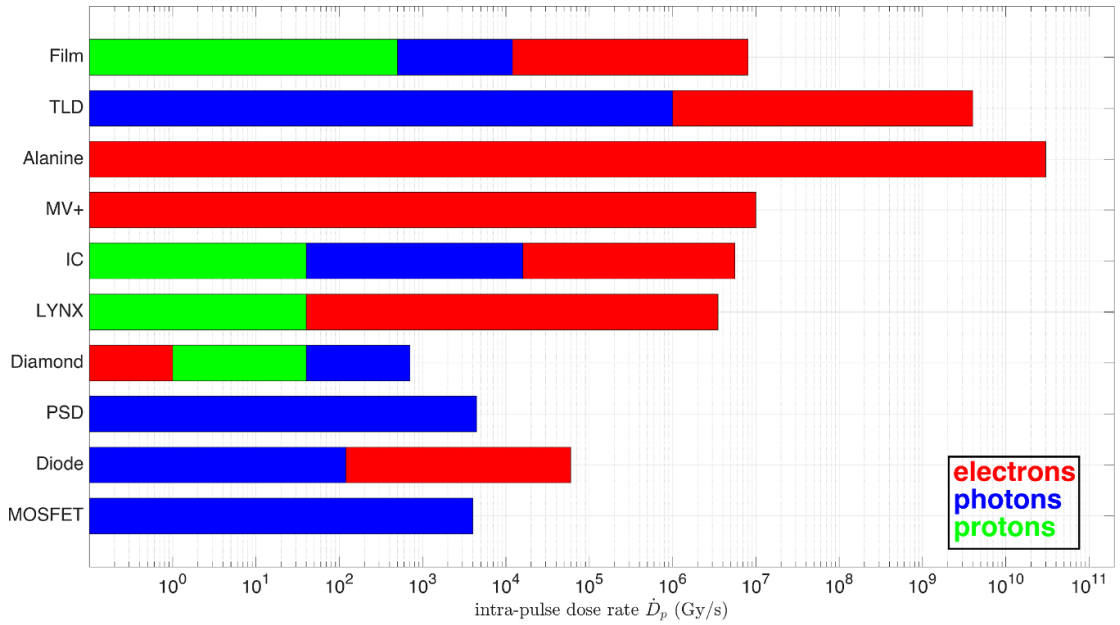

Figure 3. Detectors types which have been used for ultrahigh dose-rate irradiations along with the peak intra-pulse dose rates ($\dot{D}_P$) for which they have been successfully employed across each radiation modality (photon: γ, electron: e^-, proton: p^+). Note that the generic-named detector data corresponds to the following specific models: Film = Gafchromic EBT3; Diamond = PTW (60019) microDiamond; PSD = BC-400; Diode = X-Tream(γ), IBA EDP 20-3G (e^-). The IC data was derived from three models that are commonly employed for their respective particle modalities: e^- = PTW Advanced Markus (34045); γ = PTW PinPoint (31014); p^+ = IBA CC01.

ultrahigh dose-rates (Adamovics and Maryanski 2006); additionally, the gel boasts a high dynamic range, access to high spatial resolution (78 nm using fluorescent microscopy) (Annabell *et al* 2012) and, when paired with optical computed tomography (CT) readout (Nowais *et al* 2010), enables the acquisition of 3D dose distribution data with a linear dose-response in the range of 10–80 Gy (Doran *et al* 2013). Readout procedures for PRESAGE gels are currently compatible with rapid post-exposure optical CT readout (Skyt *et al* 2012), however challenges remain regarding the batch variability, which affects temperature and OD time-evolution, volume-dependent dose sensitivity (Jackson *et al* 2015), and spatial-resolution limitations of the optical CT system such that future developments must reliably remove these limitations before their routine application in ultrahigh dose-rate radiation fields (Doran *et al* 2013). Figure 3 and table 7 summarize detectors which have been successfully used in ultrahigh dose-rate irradiations and have shown little to no dose-rate dependence based on their successful application up to the specified values across multiple particle modalities.

3. Biology

3.1. Ultrahigh dose-rate cellular studies

Irradiation of biological samples with ultrahigh dose-rates date back to the 1960s. These experiments were done to try to answer a number of fundamental questions in radiation-biology including: the nature of lethal versus non-lethal DNA damage, direct versus indirect free radical diffusion induced DNA damage, the role of oxygen, DNA induction and repair/recovery post-irradiation, and whether any of these would be altered at ultrahigh dose-rates. Town in his 1967 Nature paper studied the survival of HeLa cervical cancer cells to 15 MeV electrons delivered as a single 1.3 μs pulse with a dose rate of $\dot{D}_P \sim 3.5 \times 10^7$ Gy s^{-1} or as two pulses

separated by 2.5 ms with $\overline{\dot{D}}$ ~1.8 × 10^4 Gy s^{-1} (Town 1967). The HeLa cell survival was similar for the two irradiation schemes up to doses of 900 rads or 9 Gy, however, for higher doses the single-pulse irradiation demonstrated a decreased radiosensitivity exhibited by a survival curve discontinuity (referred to as the 'hockey-stick') compared to two-pulse irradiation, which was then attributed to oxygen depletion during the single 1.3 μs pulse. To test this hypothesis, Town bubbled nitrogen gas into his cell samples to remove all the oxygen. The nitrogen HeLa hypoxic survival curves for the single versus two-pulse irradiation were now identical even at doses up to 4500 rads or 45 Gy supporting his oxygen depletion hypothesis. In the same year, Todd *et al* irradiated human T1 kidney cells with 10 MV x-rays with a maximum dose rate of $\dot{D}_P$ ~3 × 10^9 Gy s^{-1} in a single 30 ns pulse and compared the ultrahigh dose-rate cell survival to a ^{60}Co irradiation (Todd *et al* 1967). They did not observe any difference in cell survival for delivered doses between 2 Gy and 10.5 Gy and concluded that oxygen consumption was similar for both presented irradiation schemes. Based on their results and previous literature they estimated that a dose rate of more than 10^7 Gy s^{-1} was needed in order to deplete oxygen for total irradiation doses of 20 Gy.

In a 1969 study, Berry *et al* found no difference in survival between ultrahigh dose-rate and a ^{60}Co irradiation for Chinese hamster and HeLa cell irradiated for lower doses of <5 Gy (Berry *et al* 1969). For doses >5 Gy, both cell lines were less sensitive to the ultrahigh dose-rate of $\dot{D}_P$ of 0.3 × 10^9−2 × 10^9 Gy s^{-1} delivered as a 9 ns long pulse with a 2 MV photon beam compared to the 1 Gy min^{-1} ^{60}Co irradiation. For a 50 ns long delivery, however, the difference in survival curves between ultrahigh dose-rate and ^{60}Co delivery disappeared. Interestingly, oxygen depletion was not seen as the driving mechanism of the survival curve discontinuity. It was hypothesized that the difference in cell survival could be attributed to the initial local concentrations of radicals and radical-radical interactions.

In 1970, Nias *et al* irradiated HeLa cells with 10 MeV electrons of 10 ns pulses resulting in dose rates of $\dot{D}_P = 2 \times 10^9$ Gy s^{-1} under aerated and hypoxic conditions (Nias *et al* 1970). These authors did not find the survival curve discontinuity of the ultrahigh dose-rate delivery reported by the two aforementioned studies. It was therefore postulated that the survival curve discontinuity could be attributed to the non-uniform dose across the sample. However, Epp *et al* also suggested that another major factor that may be causing the variation in whether survival curve discontinuities occur is the uncertainty in the actual quantity of cellular oxygen present in the cells due to oxygen release from the polystyrene cell culture flasks and differences in cellular respiration (Epp *et al* 1972). Epp *et al* then demonstrated that if oxygen concentrations were carefully controlled and survival curves constructed between 0.26% and 0.91% O_2 levels these ultrahigh dose-rate inflection points can be observed that are consistent with the oxygen depletion model (Epp *et al* 1972). If ultrahigh dose-rates were indeed able to deplete oxygen in the cells then the amount of radiation-induced DNA damage would be reduced because oxygen dependent indirect free radical damage would not occur and only direct DNA damage would be observed. To test this hypothesis, early ultrahigh dose-rate investigators studied DNA damage induction and repair that manifested as chromosome breaks (two hit aberrations). In 1958 Kirby-Smith and Dolphin showed that when the dose rate of electrons and photons from a 15 MeV linear accelerator was increased from $\overline{\dot{D}}$ of 1 × 10^4 Gy s^{-1} to 4 × 10^6 Gy s^{-1} they found the percentage of two hit chromosome aberrations was reduced by 40%–50% when irradiated in air but this difference was not observed when the cells were irradiated in nitrogen under hypoxic conditions (Kirby-Smith and Dolphin 1958). Prempree *et al* also observed that when human lymphocytes were irradiated with ultrahigh dose-rates of 4.5 × 10^{10} R s^{-1} in 2 ns pulses from a 600 keV x-ray machine, the frequencies of dicentrics after 200 R were reduced from 15% to 10% and were reportedly not due to differences in chromosomal repair (Prempree *et al* 1969). Recently, Buonanno *et al* irradiated human lung fibroblast IMR90 with 4.5 MeV protons with 0.5 Gy to 10 Gy at dose rates $\dot{D}_P$ of 0.05 Gy s^{-1}, 100 Gy s^{-1}, and 1000 Gy s^{-1} at room temperature in air with a thin layer of liquid media over the cells (Buonanno *et al* 2019). They observed no differences in clonogenic survival versus dose rate but did observe a reduction in DNA double strand break (DSB) damage measured by γH2AX foci formation 30 min post-irradiation after a dose of 20 Gy delivered at 1000 Gy s^{-1} dose rate (Buonanno *et al* 2019). However, Buonanno *et al* did report a reduction in the number of premature senescent IMR90 cells measured by β-galactosidase staining appearing 1 month post-irradiation at 100 Gy s^{-1} and 1000 Gy s^{-1} versus 0.05 Gy s^{-1} and interestingly a difference in the cytokine TGF-β expression 24 h and 1 month after 20 Gy when $\dot{D}_P$was increased from 0.2 Gy s^{-1} to 1000 Gy s^{-1} (Buonanno *et al* 2019). Fouillade *et al* investigated DNA damage induction and repair after irradiation with 5.2 ± 0.2 Gy of 4.5 MeV electrons at conventional mean dose rate of $\overline{\dot{D}}$ = 0.03 Gy s^{-1} versus ultrahigh mean dose rate of $\overline{\dot{D}}$ = 40 Gy s^{-1} in two non-transformed human fibroblast cell lines MRC5 and IMR-90 and in a Non-Small Cell Human Lung Cancer cell line A549 measured by γH2AX and TRP53BP1 (53BP1) foci formation by immunofluorescence (Fouillade *et al* 2020). They observed no difference in initial radiation-induced DNA DSBs at 30 min after 5.2 Gy of irradiation measured by γH2AX foci formation but did detect statistically significant reductions in 53BP-1 foci formation after ultrahigh dose-rate irradiation

versus conventional dose rate in the two fibroblast MRC5 and IMR-90 cells that were not observed in the A549 lung cancer cells. In addition, they also reported evidence of sparing in human pulmonary bronchial epithelial cells after 4 Gy of ultrahigh mean dose rate versus conventional dose rate electrons. The reduction in 53 BP-1 foci after ultrahigh dose rate irradiation may be indicative of a different quality/type of DNA DSB being induced at ultrahigh dose rate (Fouillade *et al* 2020).

3.2. Normal tissue response

In 2014, Favaudon *et al* published a landmark study that investigated the induction of radiation-induced lung fibrosis in mice when the thoraxes of C57Blk/6J mice were irradiated with 17 Gy of ^{137}Cs gamma-rays or 4.5 MeV electrons at conventional mean dose rates of $\overline{\dot{D}} = 0.03$ Gy s^{-1} versus ultrahigh dose rates of $\overline{\dot{D}} = 40$ Gy s^{-1}, so-called FLASH-RT (Favaudon *et al* 2014). The 17 Gy dose at conventional dose rate was chosen because this has been shown by a number of investigators to induce lung fibrosis in C57Blk/6J mice by 24 weeks ~6 months post-irradiation (Franko and Sharplin 1994, Jackson *et al* 2010, Sharplin and Franko 1989a, 1989b). As expected, the majority of mice irradiated to 17 Gy at conventional dose rates did develop moderate to severe lung fibrosis at 24–36 weeks. However, after 17 Gy of FLASH-RT only a minority of the irradiated mice developed evidence of minimal to mild lung fibrosis at 36 weeks. It was not until the FLASH-RT dose of 4.5 MeV electrons was increased to 30 Gy that histological evidence of significant lung fibrosis was observed 24 weeks post-irradiation. Importantly, the investigators also went on to show that when the 4.5 MeV electrons were delivered at conventional dose rates it did induced lung fibrosis in the C57Blk/6J mice. To test whether differences in cell killing could explain their results, the authors demonstrated that 15 Gy of FLASH-RT irradiation in mice produces significantly less apoptotic death one hour post-irradiation in mouse lung tissue than 7.5 Gy of conventionally delivered gamma rays. Importantly they also showed that it took 30 Gy of FLASH-RT irradiation to obtain similar levels of apoptotic death as 7.5 Gy conventional gamma rays 1 h post-irradiation (Favaudon *et al* 2014). Fouillade *et al* have continued this lung fibrosis work with follow up studies that utilized single-cell RNA sequencing (sc-RNA-seq) analyses to identify potential changes in 16 cell subtypes such as fibroblast, immune cells, lung cell subtypes, and endothelial cells after FLASH-RT and conventional dose rate post-irradiation. Overall, after FLASH-RT they observed clear evidence of downregulation of tissue damage in irradiated lungs including; reduced cell proliferation and proinflammatory response, a reduction in persistent DNA damage measured by 53BP-1 foci in lung parenchymal cells, and reduction senescent cell clusters measured by β-galactosidase staining and expression of senescent marker genes such as P16^{INK4a} (Fouillade *et al* 2020). One of the questions which arose from these FLASH-RT studies was whether or not this was lung-tissue specific observation. To answer this question, in 2017 Montay-Gruel *et al* published a follow up study that tested whether FLASH irradiation could spare damage to mouse brain. The investigators performed 10 Gy mouse whole brain irradiations with electrons at mean dose rates from $\overline{\dot{D}}$ of 0.1 Gy s^{-1} to 500 Gy s^{-1} and also with a single pulse at $\dot{D}_P = 5.6 \times 10^6$ Gy s^{-1}. At 2 months post-irradiation, mouse memory was tested through a Novel Object Recognition Test endpoint called the Recognition Ratio (RR) (Antunes and Biala 2012, Montay-Gruel *et al* 2017). The investigators reported that 10 Gy dose delivered either as a 1.8 μs single pulse or at dose rates above 100 Gy s^{-1} or higher, preserved mouse memory i.e. the RR was similar to unirradiated controls (Montay-Gruel *et al* 2017). The protective effect on mouse memory was reduced at doses of 30 Gy s^{-1} and disappeared at dose rates below 20 Gy s^{-1}. The authors also reported that *de novo* mouse neurogenesis measured in the mouse hippocampus by incorporation of bromodeoxyuridine (BrdU) was also better preserved after FLASH-RT versus conventional radiation therapy dose rates (Montay-Gruel *et al* 2017). In a recent follow up study it was shown that FLASH mouse brain irradiation not only spared deficits in learning and memory but also reduced anxiety and depression characteristics and did not reduce extinction memory which is the ability to forget a trained relationship between an acoustic tone and a mild foot shock over time once the mild foot shock is no longer applied for example (Montay-Gruel *et al* 2019). In the same follow up study, the authors found that FLASH-RT reduced neuroinflammation by lowering the amount of astrogliosis observed and reducing the number of activated CD68 positive microglia cells in the mouse brain post-irradiation compared to conventional dose rate irradiation. Furthermore, it was observed that FLASH irradiation better preserved neuronal morphology and complexity as measured by neuronal spine density, branching, and dendritic length (Montay-Gruel *et al* 2019). In an independent study Simmons *et al* have also shown that FLASH irradiation of the mouse brain reduced cognitive deficits, dendritic spine loss, and neuroinflammation (Simmons *et al* 2019).

Vozenin *et al* went on to show skin sparing with FLASH-RT ($\overline{\dot{D}} = 300$ Gy s^{-1}) versus conventional dose rate ($\overline{\dot{D}} = 0.083$ Gy s^{-1}) electrons in a minipig at doses of 28 Gy, 31 Gy, and 34 Gy (Vozenin *et al* 2019a). Vozenin and colleagues have also reviewed and acknowledged the older literature which have also shown evidence of protection of normal tissues at ultrahigh dose-rates (Vozenin *et al* 2019b). For example, Hendry

et al showed for the endpoint mouse tail necrosis that when irradiated dose rates reached ultrahigh dose-rates (0.4 Gy per 1 μs; $\dot{D}_P = 4 \times 10^5$ Gy s^{-1}) the normalized dose to achieve 50% (ND_{50}) mouse tail necrosis was 72 Gy which was similar to the ND_{50} for clamped mouse tails with 100% hypoxic cells (Hendry *et al* 1982). They proposed this was due oxygen depletion in the mouse tissue target cells being at a relatively low oxygen concentration of 3 to 6 μM O_2 versus normal venous O_2 levels of 60 μM O_2 which would require at least 90 Gy to deplete based on measured oxygen depletion rates of 0.36 to 0.66 μM O_2 per Gy (Hendry *et al* 1982). Hornsey and Bewley also demonstrated that irradiations of the mouse intestine at ultrahigh dose-rates ($\overline{\dot{D}} \sim 17$ to 83 Gy s^{-1}) increased the $LD_{50/5}$, which is the dose of abdominal irradiation that induces 50% lethality in mice 5 d post-irradiation and death by the gastrointestinal syndrome compared to conventional dose rate irradiation (Hornsey and Bewley 1972). They hypothesized and then demonstrated that this was due to oxygen depletion and the induction of hypoxia by irradiating mice, which were made temporarily hypoxic by breathing nitrogen gas, at ultrahigh dose-rates and showing how the increase in $LD_{50/5}$ previously seen at ultrahigh dose-rates was no longer observed (Hornsey and Bewley 1972). Loo *et al* has recently made a similar observation in mice after abdominal irradiation at ultrahigh dose-rates (Loo *et al* 2017)

The use of electrons for FLASH-RT normal tissue studies in small animals has advantages in terms of the uniformity of the depth dose profile with the entrance dose being greater than 95% of the dose maximum for 20 MeV electrons. Since most of the above normal tissue studies were performed with electrons, the next question which arose in the field was whether FLASH-RT irradiation with x-rays would also produce sparing of normal tissue versus irradiation at conventional dose rates. Montay-Gruel *et al* demonstrated that ultrahigh dose-rate x-ray FLASH-RT irradiations of whole mouse brains of C57Bl/6J mice with 10 Gy of synchrotron x-rays produced at a mean dose rate of $\overline{\dot{D}} = 37$ Gy s^{-1} also spared cognitive deficits when the novel object recognition test was performed at 2 and 6 months post-irradiation compared to mice that were irradiated with 10 Gy at a conventional dose rate of 0.05 Gy s^{-1}. The authors also demonstrated the FLASH-RT x-rays also better preserved *de novo* mouse neurogenesis in the mouse hippocampus and reduced astrogliosis versus irradiation at conventional radiation therapy dose rates (Montay-Gruel *et al* 2018).

Diffenderfer *et al* have designed and implemented a proton FLASH-RT system that utilizes double scattered FLASH protons with CT guidance (Diffenderfer *et al* 2020). The proton FLASH-RT mean dose rate was $\overline{\dot{D}} = 78 \pm 9$ Gy s^{-1} and the conventional dose rate was 0.9 ± 0.08 Gy s^{-1}. They showed that whole abdominal irradiation of C57BL/6J mice with 15 Gy of FLASH protons spared gut damage measured by the intestinal crypt cell assay versus protons delivered at conventional dose rate. They also reported that 18 Gy of FLASH-RT protons induced significantly less intestinal fibrosis than protons delivered at conventional dose rate (Diffenderfer *et al* 2020).

While a number of investigators have observed FLASH-RT sparing effects of normal tissue, Venkatesulu *et al* did not observe FLASH-RT normal tissue protection (Venkatesulu *et al* 2019). They utilized a modified Varian 2100 to deliver 20 MeV electrons at a mean dose rate of $\overline{\dot{D}} = 35$ Gy s^{-1} versus conventional irradiation with a Varian True Beam at a conventional dose rate of 0.1 Gy s^{-1}. They did not observe FLASH-RT normal tissue sparing for gastrointestinal toxicity versus conventional dose rate electrons after a single fraction of 16 Gy to the whole abdominal region in BALB/c mice. In addition, they did not observe sparing of radiation-induced lymphopenia after splenic irradiation with 1 Gy daily fractions for five consecutive days or after cardiac irradiation with a 5 Gy single fraction in male C57BL/6 mice (Venkatesulu *et al* 2019). Further experiments at higher FLASH-RT dose rates with this system may be required to better understand these observations.

3.3. Tumor tissue response

The excitement for normal tissue sparing by ultrahigh dose-rate delivery of electrons, x-rays, and protons has been greatly enhanced by the observation that FLASH-RT does not appear to reduce tumor response *in vivo* (Favaudon *et al* 2014) compared to conventional RT which would potentially greatly benefit the therapeutic ratio. Favaudon *et al* found that ultrahigh dose-rate 4.5 MeV electrons ($\overline{\dot{D}} =$ 60 Gy s^{-1}), delivered in two 27 Gy fractions or 20 Gy delivered in one fraction, were isoeffective at inducing tumor growth delay when compared with conventional dose-rate irradiations, which included two 17 Gy fractions of ^{137}Cs γ-rays delivered at 0.03 Gy s^{-1} or a single 19.5 Gy fraction of 200 kV x-rays at 0.012 Gy s^{-1}. This isoeffect was demonstrated in human breast cancer HBCx-12 A cells and in human head and neck cancer Hep-2 cells growing subcutaneously as tumor xenographs in nude mice (Favaudon *et al* 2014). In addition, when the single fraction dose of electron FLASH-RT was escalated to 25 Gy, tumor growth was completely suppressed even 40 d post-irradiation. Importantly, the authors performed syngeneic, orthotopic tumor studies in the C57BL/6J mouse model by injecting TC-1 mouse lung carcinoma cells into the lung. They showed that bilateral thorax irradiations of these tumor bearing mice with 15 Gy of 4.5 MeV electron FLASH-RT delivered at $\overline{\dot{D}} =$ 60 Gy s^{-1} and with 15 Gy of 4.5 MeV electrons delivered at the conventional dose rate of

0.03 Gy s^{-1} resulted in isoeffective and very similar tumor growth delay. In addition, the authors performed dose escalation studies with 23 Gy and 28 Gy of 4.5 MeV electrons FLASH-RT and measured tumor bearing C57BL/6J mouse survival by Kaplan-Meier analysis and showed that 60% of 28 Gy FLASH-RT irradiated tumor bearing mice were alive and tumor free two months post-irradiation with no evidence of lung fibrosis, which would not be possible with 28 Gy of conventional dose rate electrons (Favaudon *et al* 2014). These orthotopic mouse tumor studies in the C57BL/6J mouse model were also important because they have an intact immune system unlike the nude mutant mouse model which can grow human tumors because their immune system has been genetically disabled (Fogh *et al* 1977).

Diffenderfer *et al* performed proton FLASH-RT and irradiated 10 d old flank tumors in the C57BL/6J mice induced by injecting MH641905 KPC pancreatic cancer cells subcutaneously. The authors then irradiated the tumors with 12 Gy or 18 Gy of FLASH-RT $\bar{\dot{D}} = 78 \pm 9$ Gy s^{-1} or conventional dose rate of 0.9 ± 0.08 Gy s^{-1} protons and observed that tumor growth delay was similar for FLASH-RT and conventional dose rate proton irradiations suggesting an improved benefit to the therapeutic ratio (Diffenderfer *et al* 2020).

Bourhis *et al* also recently treated H454 orthotopic GBM brain tumors in nude mice with 10 Gy single fraction, 3 fractions of 8 Gy, and five fractions of 5 Gy delivered as electron FLASH-RT in one 1.8×10^{-6} s pulse at $\dot{D}_P = \ 5.5 \times 10^6$ Gy s^{-1} or at conventional (0.1 Gy s^{-1}) dose rates with 1 d between fractions (Bourhis *et al* 2019a). This data supported that daily fractions of FLASH-RT and conventional dose rate RT induced similar tumor growth delay suggesting that fractionation of FLASH-RT is possible without compromising tumor treatment (Bourhis *et al* 2019a).

In 2018 Vozenin *et al* published a small dose escalation trial, in which they treated six cats with squamous cell carcinomas on their noses with single electron FLASH-RT dose of 25 Gy to 41 Gy (Vozenin *et al* 2019a). Five out of the six cats had complete and durable responses 16 months post-irradiation with some normal tissue toxicity that healed and with no evidence of late toxicity more than a year post-irradiation (Vozenin *et al* 2019a). In 2019 Bourhis *et al* successfully treated a 3.5 cm lesion on right forearm of a patient with CD30+ cutaneous T-cell lymphoma with 15 Gy of 5.6 MeV FLASH-RT electrons delivered in 90 ms that had repeatedly failed standard radiation treatment. The tumor responded and shrank beginning around 10 d post-irradiation and completely responded 36 d post-irradiation, which was durable for 5 months (Bourhis *et al* 2019b).

A comprehensive summary of the above-mentioned FLASH-RT normal-tissue and tumor studies to date, including relevant treatment delivery parameters (dose-rates, total dose, anesthesia), the type of biological system and tissue types, and the chosen endpoints, are included in table 8.

3.4. Proposed mechanisms of FLASH cells, normal tissues, and tumors

When taken together, all of the above biology data suggests that ultrahigh dose-rate sparing in cells or normal tissues appears to be due in part to oxygen depletion, altered reactive oxygen species, and the onset of a transient protective hypoxia. Montay-Gruel *et al* directly tested this hypothesis in the mouse brain by showing that increasing the local concentration of O_2 by a factor of two (from in the mouse brain by having the mice breath carbogen was able to negate the FLASH sparing on neurocognition (Montay-Gruel *et al* 2019). They also performed radiation chemistry studies and clearly demonstrated reduced reactive oxygen species in solutions irradiated at FLASH versus conventional dose rates (Montay-Gruel *et al* 2019). Careful analysis of the cellular studies performed at ultrahigh dose-rates also shows that doses required to see this protective hypoxia required the investigators to carefully control and reduce the oxygen concentrations to levels where the FLASH delivered radiation dose could remove all the oxygen (Vozenin *et al* 2019b). Vozenin *et al* recently stated that it is not surprising that there are several publications that perform ultrahigh dose-rate/FLASH irradiations with electrons, protons, and x-rays, of cells *in vitro* at 21% O_2 and observed no FLASH effects, even at doses up to 19 Gy. This is because experimental data and calculations have estimated that radiation depletes O_2 at 0.44 μM Gy^{-1} and you would require 90 Gy to deplete that amount of oxygen *in vitro* (Vozenin *et al* 2019b). Therefore, it is important for investigators to remember that when designing *in vitro* cell biology ultrahigh dose-rate experiments they keep oxygen levels in the range found in most normal tissues which range from 4% to 7.5% with a mean level of ~5% O_2, ~38 mmHg pO_2, or 25 μM O_2 (Mckeown 2014). Pratx and Kapp have also proposed that when discussing FLASH-RT protection of normal tissues it is important to keep in mind that stem cell niches in normal tissues are at relatively low oxygen levels between 1%–7% O_2, 8 to 60 mmHg pO_2, or ~15 to 35 μM O_2 (Pratx and Kapp 2019a, 2019b). Adrian *et al* have recently confirmed that when prostate cells are irradiated *in vitro* at oxygen concentrations from 1.6%–20% with 10 MeV electrons at dose rates of $\bar{\dot{D}} = 600$ Gy s^{-1} versus conventional dose rate of 0.23 Gy s^{-1} that ultrahigh dose-rate sparing was oxygen dependent and due to oxygen depletion (Adrian *et al* 2020).

Table 8. Summary of FLASH-RT normal tissue and tumor studies. ND = not done.

Energy & Particle Type	$\bar{\dot{D}}(\mathbf{Gy\,s^{-1}})$	Total Dose (Gy)	Species/ Strain	Normal Tissue	Normal Tissue Protection/ Endpoint	Tumor Type	Isoeffective Tumor Kill	Anesthesia	Ref.
4.5 MeV electrons	⩾40	7.5,15, 17, 30	Mice/ C57Blk6 Swiss *nu/nu* mice	Lung	Yes/ ↓Fibrosis	Breast & Head & Neck CA TC-1	Yes	Ketamine-xylazine	(Favaudon *et al* 2014)
4.5 MeV electrons	⩾40	17	Mice/ C57Blk6 Mice/Terc/	Lung	Yes/ ↓Cell and DNA damage and ↓inflammation makers	ND	ND	Isoflurane	(Fouillade *et al* 2020)
4.5 & 6 MeV electrons	⩾100	10	Mice/ C57Blk/6J	Brain	Yes/↑Spatial memory, ↑Hippocampal Neurogenesis, ↓Astrogliosis	ND	ND	Isoflurane	(Montay-Gruel *et al* 2017)
4.5 & 6 MeV electrons	⩾100	10,12	Mice/ C57Blk/6J	Brain	Yes/ ↑Neurocognition, ↓Neuro-inflammation ↓Anxiety, Preserved Neuronal morphology and complexity, Role of O_2 depletion tested	ND	ND	Isoflurane	(Montay-Gruel *et al* 2019)

Table 8. Continued

Energy & Particle Type	$\bar{\dot{D}}$(Gy s^{-1})	Total Dose (Gy)	Species/ Strain	Normal Tissue	Normal Tissue Protection/ Endpoint	Tumor Type	Isoeffective Tumor Kill	Anesthesia	Ref.
16 or 20 MeV electrons	200 or 300	30	Mice/ C57Blk/6J	Brain	Yes/↑Spatial memory,↑Spine & dendritic density, ↓Microglial activation, ↓ Proinflammatory Cytokines/neuroinflammation	ND	ND	Ketamine	(Simmons *et al* 2019) (Lempart *et al* 2019)
4.5 & 6 MeV electrons	300	28, 31, 34	Minipig/ Goettingen	Skin	Yes/ ↓Skin Fibrosis ↓ hair follicle	ND	ND	General anesthesia	(Vozenin *et al* 2019a)
4.5 & 6 MeV electrons	300	25, 27, 28, 31, 34, 41	Cat	Nasal skin	Yes/Depilation was noted, no late skin toxicities	Squamous cell CA Nasal plenum	Yes Complete Response	General anesthesia	(Vozenin *et al* 2019a)
10 Mev electrons	0.4 Gy μs^{-1}	72	Mice/B6D2F1	50% Tail necrosis	Yes/ ↓Tail Necrosis due to O_2 depletion	ND	ND	None	(Hendry *et al* 1982)
7 MeV electrons	17 to 83	10 to 17	Mice/TO strain	Intestine	Yes/↑in mouse LD50/5 from 11.9 Gy to 13.4 Gy due to O_2 depletion	ND	ND	Nembutal	(Hornsey and Bewley 1971)

Table 8. Continued

Energy & Particle Type	$\bar{D}$(Gy s^{-1})	Total Dose (Gy)	Species/ Strain	Normal Tissue	Normal Tissue Protection/ Endpoint	Tumor Type	Isoeffective Tumor Kill	Anesthesia	Ref.
16 or 20 MeV electrons	70, 200	10 to 22	Mice/C57Blk/6J	Intestine	Yes//↑in mouse LD50/5 from 14.7 Gy to 17.5 Gy	ND	ND	Ketamine	(Loo *et al* 2017)
102 keV X-rays synchrotron	37	10	Mice/C57Blk/6J	Brain	Yes/↑Spatial memory, ↑Hippocampal Neurogenesis, ↓Astrogliosis	ND	ND	Isoflurane	(Montay-Gruel *et al* 2018)
4.5 & 6 MeV electrons	1 pulse 5.5×10^6	10 3 × 8 5 × 5	Mice/Nude C57Blk/6J	Subcutaneous & orthotopic brain	ND Yes	U87 & H454 GBM brain tumors	Yes	Isoflurane	(Bourhis *et al* 2019a)
5.6 MeV electrons	1 pulse 90 ms	15 Gy	Human	Skin	Yes/No early or late skin toxicities	Cutaneous Lymphoma	Yes Complete Response	None	(Bourhis *et al* 2019b)
230 MeV protons	78	12, 15, 18	Mice/ C57Blk/6J	Intestine	Yes/↑ crypt regeneration ↓ fibrosis	KPC PanCa	Yes	Isoflurane	(Diffenderfer *et al* 2020)
29 MeV electrons	35	16,10 (2 Gy d^{-1}) (1 Gy d^{-1})	Mice/BALB/c Mice/ C57Blk/6J	Intestine Lymphopenia	No/↑cell kill No/↑ cell kill	ND	ND	?	(Venkatesulu *et al* 2019)

Bourhis *et al* have stated that analysis of the FLASH-RT literature has now shown that the most important physical radiation parameters for the FLASH-RT normal tissue protection based on oxygen depletion are a combination of dose, dose-rate within the pulse, and keeping the overall irradiation time to <200 ms (Bourhis *et al* 2019a). Other explanations for the FLASH normal tissue protection have been discussed including reduced inflammation and altered cytokine signaling post-irradiation (Buonanno *et al* 2019, Montay-Gruel *et al* 2019, Fouillade *et al* 2020). However, how FLASH-RT can spare normal tissue but remain isoeffective for tumor response was unclear. Spitz *et al* has recently argued that careful experimental investigation of the radiation biophysics, free radical biology, and tumor and normal tissue redox metabolism will be required to help explain the counter intuitive aspects of FLASH-RT normal tissue protection and isoeffective tumor response versus conventional dose rate radiation delivery (Spitz *et al* 2019). They used biophysical and free radical biochemical modeling to demonstrate that a 10 Gy FLASH-RT dose produces sufficient yields of free radicals, organic peroxyl ($ROO^{\cdot}$) radicals and organic hydroperoxides (ROOH), and aqueous electrons (e^{-}_{aq}) to consume 25 μM O_2, i.e. all of the local tissue O_2 and produce transient hypoxia. The authors argued that differences between normal and cancer cell metabolism, such as increased labile Fe in cancer cells and lower pro-oxidant burdens in normal cells, result in normal tissue sparing but isoeffective tumor killing. Essentially, FLASH irradiation converts all the O_2 in both cancer and normal cells to hydroperoxides, however the normal cells have a greater ability to removes these toxic hydroperoxides by antioxidant pathways, but the excess Fe in cancer cells induces Fenton reactions and peroxidation reactions that slows the removal of these toxic compounds that result in sparing of normal cells but more killing in cancer cells (Spitz *et al* 2019). Spitz and colleagues have therefore provided the FLASH field with a theoretical hypothesis that can be rigorously tested experimentally with biochemical and cellular *in vitro* models, as well as *in vivo* tissue and tumor models that can take into account the complex biochemical milieu of cells and tissues.

4. Clinical translation and future prospects

To date, a number of FLASH *in vitro* and *in vivo* studies and one veterinary and patient study have been published. However, only small targets of 2–3.5 cm in size located at shallow depths in tissue have been successfully irradiated with FLASH using either low-energy electron and photon beams, each with limited tissue penetration. The majority of FLASH experiments have been performed using electron beams of low energy, between 4.5 MeV to 9 MeV, with corresponding ranges in tissue of ~2 cm to ~4.5 cm (i.e. Kinetron and Oriatron respectively). However, higher energy 20 MeV electrons, with a range in tissue of ~10 cm (Clinac 21EX), have also showed a positive FLASH effect (Simmons *et al* 2019). With respect to photon FLASH, the ESRF 102 keV synchrotron beam is characterized by a steep dose fall off with depth in tissue—the percentage depth dose at 5 cm depth is 50% (Martínez-Rovira *et al* 2012). The aforementioned beams are clearly sufficient for preclinical treatments and treatments of small shallow targets, however clinical tumors typically deep-seated and occupy larger volumes within the patient body. As a result, a clinical translation of FLASH-RT will only become feasible with the application of higher-energy beams, as is discussed below.

4.1. Treatment machines

Currently, proton therapy lends itself as the most readily available modality for clinical implementation of FLASH. As mentioned in section 3.2, the IBA Proteus system has been used to deliver FLASH with doubly-scattered proton beam (Diffenderfer *et al* 2020). For treatments of large, clinically relevant targets, pencil beam scanning is necessary; unfortunately, scanned proton pencil beams have not yet demonstrated a capacity to trigger the FLASH effect. While proton pencil beams can already be used to deliver ultrahigh dose-rates to relevant depths within patients' bodies, the prevailing limitation of proton FLASH-RT relates to how pencil beams must be scanned to cover a large area. Moreover, the proton beam energy must be changed in order to irradiate sizable volumes, which takes time and decreases the treatment mean dose rate. Varian Medical Systems recognized the role of proton systems in FLASH RT and founded the FLASHForward consortium to build its evidence-based introduction [5].

The concept of electronically-steered VHEE beams synergizes well with the goals of FLASH-RT, namely rapid (<500 ms) treatment delivery at ultrahigh dose-rates and alleviation of the high entrance doses made possible through multi-directional delivery. VHEE treatments naturally benefit from more rapid dose delivery at clinically-relevant depths relative to photons and, when paired with electromagnetic beam scanning (Papiez *et al* 2002, Bazalova-Carter *et al* 2015b), could support delivery of rapid, multi-directional electron FLASH treatments. Due to the inclusion of multiple beam directions and the resulting dose

[5] www.varian.com/about-varian/research/flashforward-consortium.

conformality, the VHEE dose rate to normal tissues would likely be below the FLASH threshold. Therefore, in order to reach the ultrahigh dose-rate in normal tissue, the VHEE beam current should be increased.

Presently, the PHASER system stands as an attractive candidate for realizing the clinical translation of image-guided FLASH-RT on a compact platform. The system will be capable of ultra-fast, multi-directional, and unique intensity-modulated treatments using electron energies of 100–200 MeV (Maxim *et al* 2019b). Sixteen fast-switching (300 ns) stationary beam lines will provide non-coplanar IMRT FLASH delivery without need for gantry rotation, thereby accommodating the <500 ms irradiation time scales required for FLASH-RT. IMRT capabilities are proposed on the basis of either pencil beam scanning or by way of photocathode-derived spatially-fractionated source images which may be accelerated in unison. For its initial application as an ultrahigh dose-rate photon source, the PHASER will use the sixteen 10 MV high-gradient DRAGON linacs (see section 2.1.1.2) and a specialized Bremsstrahlung target and collimator (SPHINX). IMRT is proposed through a combination of electronic beam scanning and post-target collimation, which will facilitate grid-like spatial intensity-modulation. Altogether, the PHASER system may offer a compact and economical solution for FLASH-RT with integrated image-guidance and IMRT capabilities for both MV photons and, eventually, VHEE electrons.

Online imaging will be a crucial aspect for all FLASH-RT machines. Since entire fractions, or at least treatment dose for single-fraction treatments, will be delivered in sub-second intervals, it will be critical to localize the target in a patient image just prior the treatment. Ideally, the FLASH treatment machine should be capable of fast online volumetric imaging. Assuming an achievable delay of 10 ms between the end of imaging and treatment, and a maximum tumor motion speed of 72.6 mm s^{-1} detected for a lung cancer patient (Shirato *et al* 2006), the tumor would move by 0.7 mm after imaging and before treatment. Such motion should be adequately captured in the planning target volume, assuming the imaging is performed quickly and that no tumor motion occurs during the short (<50 ms) imaging session. Motion would result in blurry images, which could potentially be recognized and prompt a repetition of the imaging session.

Fast volumetric imaging could be achieved by integrating a CT scanner, such as suggested by (Cherry Kemmerling *et al* 2015) or by accommodating an electron-beam CT scanner capable of 10 ms/slice imaging time (Akai 1989). Other online imaging solutions could be considered, such as by integrating magnetic resonance imaging (MRI) or a positron emission tomography (PET) scanner for photon FLASH machines. While it would be a major technological challenge, an MRI-guided FLASH linac could be similar in design to MRI-linac systems (Raaymakers *et al* 2009), except it would contain a number of linacs that could deliver conformal radiation from multiple directions simultaneously. Similarly, the RefleXion X1 system developed for emission-guided RT (Mazin 2017) could be modified for the delivery of FLASH under PET guidance if a number of linacs were used instead of one. One would have to carefully design such a machine with a number of linacs constrained by the machine geometry. The linacs would have to employ a liquid bremsstrahlung target, as Wang *et al* using a solid tungsten target limits the dose rate to 1.16 Gy s^{-1} per linac at 100 cm SSD (Wang *et al* 2017). Another alternative would be to use a number of VHEE linacs, as proposed for the PHASER project (Maxim *et al* 2019b).

4.2. Treatment planning

It is currently not clear whether the entire treatment dose has to be delivered in a sub-second interval in order to maintain the FLASH protective effect of normal tissue. Montay-Gruel *et al* (2018) in their whole-brain FLASH study performed with a thin 50 μm synchrotron x-ray beam swept across a mouse brain in 0.27 s suggest that not only temporal but also spatial fractionation may be a factor in normal tissue protection. The in-slice dose rate of 12 000 Gy s^{-1} resulted in mean dose rate of 37 Gy s^{-1} to the brain, which is thought to be at or slightly below the threshold for the FLASH protective effect in normal tissues. However, compared to conventional irradiations, animals irradiated with FLASH exhibited higher memory and hippocampal cell division preservation and reduced induction of reactive astroglyosis. Treatment planning will therefore play an important role in FLASH-RT and both temporal and spatial dose distribution will have to be considered in treatment plan evaluation. Additionally, biological planning should be implemented to reflect the NTCP and possibly TCP response as a function of planned dose rate.

Two ultrahigh dose-rate proton therapy planning studies have been published to date. Van de Water *et al* have presented that, with a number of assumptions including ignoring the gantry rotation time and dead time between spots, ultrahigh dose-rate proton irradiations of head and neck patients might in principle be possible with pencil beam scanning at Paul Scherrer Institute (van de Water *et al* 2019). Van Marlen *et al* explored treatment planning for proton beam scanning in transmission delivery mode (with the Bragg peak outside of the patient body) for stereotactic lung patients using non-coplanar beams. While the lung plans were comparable to VMAT plans, they concluded that it was impossible to deliver ultrahigh dose-rate RT to the entire irradiated volume, and even for a high pencil beam dose rate of 360 Gy s^{-1}, only 75% of the entire dose was delivered with ultrahigh dose-rates (van Marlen *et al* 2019). Additionally, a more appropriate

metric reflecting FLASH-capability of the generated plans would have been the fraction of normal tissue rather than the fraction of all irradiated tissue irradiated with ultrahigh dose-rate.

In 2015, a Stanford group investigated treatment planning for RT with VHEE, at the time to deliver RT in a fast manner to avoid the need for tumor tracking (Bazalova-Carter *et al* 2015b). They concluded that a dose rate of 117 Gy s^{-1} could be achieved for a 100 MeV scanning electron pencil beam, if electromagnetic steering of the electron beam is ignored. This is considered to be a FLASH-compatible dose rate and thus VHEE RT together with the PHASER system could become another clinically-feasible FLASH-RT modality.

Despite the enormous research effort and involvement of industry, a wide clinical translation of FLASH therapy still remains uncertain. Here we list a number of questions that must be addressed before this novel delivery technique is implemented in the clinic.

(a) What machines will be capable of delivering ultrahigh dose-rate RT to large, clinically relevant, deep-seated targets?
(b) How will online imaging be implemented to ensure accurate dose delivery performed?
(c) How will online treatment beam dosimetry be performed?
(d) Does FLASH-RT result in TCP comparable to conventional RT for all tumors?
(e) What are the required temporal and spatial beam properties resulting in FLASH effect sparing healthy tissues and maintaining tumor control?
(f) Will treatment planning have to take into account the temporal and spatial characteristics of the dose distributions? If so, how will this be achieved?
(g) How will FLASH-RT be fractionated? Will a single fraction result in acceptable NTCP or will multiple fractions still be necessary?

While extensive FLASH research is currently being performed to answer these questions, there is at present no clear picture of how clinical translation will be implemented.

5. Conclusions

Ultrahigh dose-rate FLASH radiation therapy appears to be an extremely promising treatment modality for cancer patients and has generated much excitement in the radiation oncology community over the past few years. Here we present a summary of existing and prospectively FLASH-capable radiation sources, the challenges and possible solutions for FLASH dosimetry, along with an evaluation of radiobiological findings so far and of avenues towards clinical translation of FLASH-RT. While the published evidence of improved normal tissue sparing following FLASH therapy is no less than impressive, not all recent FLASH studies have resulted in such a clear-cut picture. It is important to note that many questions remain regarding the overall impact of FLASH-RT, its mechanisms and clinical feasibility and it has become clear that one of the major goals of radiation therapy today is to unfold the mystery of FLASH.

Acknowledgments

We would like to thank Yolanda Prezado and Cornelia Hoehr for their help with beam parameters achieved with the ESFR synchrotron and TRIUMF beamlines, respectively. This work was partly supported by NSERC Discovery Grant, the Canada Research Chair program and the New Frontiers in Research Fund.

ORCID iD

Nolan Esplen https://orcid.org/0000-0002-8347-8653

References

Abel E 2019 Varian proton machine parameters
Adamovics J and Maryanski M J 2006 Characterisation of PRESAGE™: a new 3-D radiochromic solid polymer dosemeter for ionising radiation *Radiat. Prot. Dosim.* **120** 107–12
Adrian G, Konradsson E, Lempart M, Bäck S, Ceberg C and Petersson K 2020 The FLASH effect depends on oxygen concentration *Br. J. Radiol.* **92** 20190702
Agostinelli S, Garelli S, Piergentili M and Foppiano F 2008 Response to high-energy photons of PTW31014 PinPoint ion chamber with a central aluminum electrode *Med. Phys.* **35** 3293–301
Akai M 1989 Ultrahigh speed X-ray CT scanner Google Patents
Aldosary G, Safigholi H, Song W, Seuntjens J and Sarfehnia A 2017 Polarity and ion recombination corrections in continuous and pulsed beams for ionization chambers with high Z chamber walls *Phys. Medica* **35** 102–9

Almaviva S, Marinelli M, Milani E, Prestopino G, Tucciarone A, Verona C, Verona-Rinati G, Angelone M, Pillon M and Dolbnya I 2010 Chemical vapor deposition diamond based multilayered radiation detector: physical analysis of detection properties *J. Appl. Phys.* **107** 014511

Almond P R, Biggs P J, Coursey B, Hanson W, Huq M S, Nath R and Rogers D 1999 AAPM's TG-51 protocol for clinical reference dosimetry of high-energy photon and electron beams *Med. Phys.* **26** 1847–70

Andreo P, Burns D T, Hohlfeld K, Huq M S, Kanai T, Laitano F, Smyth V and Vynckier S 2000 Absorbed dose determination in external beam radiotherapy: an international code of practice for dosimetry based on standards of absorbed dose to water *Vienna (Austria): IAEA Technical Report Series*

Annabell N, Yagi N, Umetani K, Wong C and Geso M 2012 Evaluating the peak-to-valley dose ratio of synchrotron microbeams using PRESAGE fluorescence *J. Synchrotron Radiat.* **19** 332–9

Antunes M and Biala G 2012 The novel object recognition memory: neurobiology, test procedure, and its modifications *Cogn. Process.* **13** 93–110

Archer J, Li E, Davis J, Cameron M, Rosenfeld A and Lerch M 2019 High spatial resolution scintillator dosimetry of synchrotron microbeams *Sci. Rep.* **9** 1–7

Arjomandy B, Tailor R, Anand A, Sahoo N, Gillin M, Prado K and Vicic M 2010 Energy dependence and dose response of Gafchromic EBT2 film over a wide range of photon, electron, and proton beam energies *Med. Phys.* **37** 1942–7

Arjomandy B, Tailor R, Zhao L and Devic S 2012 EBT2 film as a depth-dose measurement tool for radiotherapy beams over a wide range of energies and modalities *Med. Phys.* **39** 912–21

Auer S, Hable V, Greubel C, Drexler G A, Schmid T E, Belka C, Dollinger G and Friedl A A 2011 Survival of tumor cells after proton irradiation with ultra-high dose rates *Radiat. Oncol.* **6** 2–9

Bartzsch S and Oelfke U 2017 Line focus x-ray tubes—a new concept to produce high brilliance x-rays *Phys. Med. Biol.* **62** 8600–15

Bartzsch S and Tag J 2014 Microbeam radiation therapy—physical and biological aspects of a new cancer therapy and development of a treatment planning system *PhD Diss.*

Bayart E, Flacco A, Delmas O, Pommarel L, Levy D, Cavallone M, Megnin-Chanet F, Deutsch E and Malka V 2019 Fast dose fractionation using ultra-short laser accelerated proton pulses can increase cancer cell mortality, which relies on functional PARP1 protein *Sci. Rep.* **9** 1–10

Bazalova-Carter M and Esplen N 2019 On the capabilities of conventional x-ray tubes to deliver ultra-high (FLASH) dose rates *Med. Phys.* **46** 5690–5

Bazalova-Carter M, Liu M, Palma B, Dunning M, Mccormick D, Hemsing E, Nelson J, Jobe K, Colby E and Koong A C 2015a Comparison of film measurements and Monte Carlo simulations of dose delivered with very high-energy electron beams in a polystyrene phantom *Med. Phys.* **42** 1606–13

Bazalova-Carter M, Qu B, Palma B, Hårdemark B, Hynning E, Jensen C, Maxim P G and Loo Jr B W 2015b Treatment planning for radiotherapy with very high-energy electron beams and comparison of VHEE and VMAT plans *Med. Phys.* **42** 2615–25

Beaulieu L and Beddar S 2016 Review of plastic and liquid scintillation dosimetry for photon, electron, and proton therapy *Phys. Med. Biol.* **61** R305

Beddar A, Mackie T and Attix F 1992 Water-equivalent plastic scintillation detectors for high-energy beam dosimetry: I. Physical characteristics and theoretical considerations *Phys. Med. Biol.* **37** 1883

Berry R J, Hall E J, Forster D W, Storr T H and Goodman M J 1969 Survival of mammalian cells exposed to X rays at ultra-high dose-rates *Br. J. Radiol.* **42** 102–7

Beyreuther E *et al* 2019a Research facility for radiobiological studies at the university proton therapy dresden *Int. J. Part. Ther.* **5** 172–82

Beyreuther E, Brand M, Hans S, Hideghéty K, Karsch L, Leßmann E, Schürer M, Szabó E R and Pawelke J 2019b Feasibility of proton FLASH effect tested by zebrafish embryo irradiation *Radiother. Oncol.* **139** 46–50

Beyreuther E *et al* 2010 Establishment of technical prerequisites for cell irradiation experiments with laser-accelerated electrons *Med. Phys.* **37** 1392–400

Beyreuther E, Karsch L, Laschinsky L, Leßmann E, Naumburger D, Oppelt M, Richter C, Schürer M, Woithe J and Pawelke J 2015 Radiobiological response to ultra-short pulsed megavoltage electron beams of ultra-high pulse dose rate *Int. J. Radiat. Biol.* **91** 643–52

Blackmore E 2019 TRIUMF proton machine parameters

Bloch C 2019 IBA proton machine parameters

Boag J 1966 Ionization chambers *Radiation Dosimetry* eds F H Attix and W C Roesch (New York: Academic) vol **2** pp 1–72

Boag J W and Currant J 1980 Current collection and ionic recombination in small cylindrical ionization chambers exposed to pulsed radiation *Br. J. Radiol.* **53** 471–8

Boag J W, Hochhäuser E and Balk O A 1996 The effect of free-electron collection on the recombination correction to ionization measurements of pulsed radiation *Phys. Med. Biol.* **41** 885–97

Boag J W and Wilson T 1952 The saturation curve at high ionization intensity *Br. J. Appl. Phys.* **3** 222–9

Borca V C, Pasquino M, Russo G, Grosso P, Cante D, Sciacero P, Girelli G, La Porta M R and Tofani S 2013 Dosimetric characterization and use of GAFCHROMIC EBT3 film for IMRT dose verification *J. Appl. Clin. Med. Phys.* **14** 158–71

Bouchet L 2019 Mevion proton machine parameters

Boudou C, Troprès I, Rousseau J, Lamalle L, Adam J F, Estève F and Elleaume H 2007 Polymer gel dosimetry for synchrotron stereotactic radiotherapy and iodine dose-enhancement measurements *Phys. Med. Biol.* **52** 4881–92

Bourhis J *et al* 2019a Clinical translation of FLASH radiotherapy: why and how? *Radiother. Oncol.* **139** 11–17

Bourhis J *et al* 2019b Treatment of a first patient with FLASH-radiotherapy *Radiother. Oncol.* **139** 18–22

Bräuer-Krisch E *et al* 2015 Medical physics aspects of the synchrotron radiation therapies: microbeam radiation therapy (MRT) and synchrotron stereotactic radiotherapy (SSRT) *Phys. Medica* **31** 568–83

Bräuer-Krisch E, Bravin A, Lerch M, Rosenfeld A, Stepanek J, Di Michiel M and Laissue J A 2003 MOSFET dosimetry for microbeam radiation therapy at the European synchrotron radiation facility *Med. Phys.* **30** 583–9

Bräuer-Krisch E, Siegbahn E A and Bravin A 2009 GafChromic(R) film measurements for microbeam radiation therapy (MRT) *FMBE Proc.* **25** pp 174–7

Breitkreutz D Y, Renaud M-A, Weil M D, Zavgorodni S, Han J, Baxter H, Seuntjens J, Song S, Boyd D and Bazalova-Carter M 2019 Monte Carlo calculated kilovoltage x-ray arc therapy plans for three lung cancer patients *Biomed. Phys. Eng. Express* **5** 065022

Brown T A D, Hogstrom K R, Alvarez D, Ii K L M and Ham K 2012 Dose-response curve of EBT, EBT2, and EBT3 radiochromic films to synchrotron-produced monochromatic x-ray beams *Med. Phys.* **39** 7412–7

Bruggmoser G, Saum R, Schmachtenberg A, Schmid F and Schüle E 2007 Determination of the recombination correction factor kS for some specific plane-parallel and cylindrical ionization chambers in pulsed photon and electron beams *Phys. Med. Biol.* **52** N35–50
Bucciolini M *et al* 2005 Diamond dosimetry: outcomes of the CANDIDO and CONRAD INFN projects *Nucl. Instrum. Methods Phys. Res.* A **552** 189–96
Bucciolini M, Buonamici F B, Mazzocchi S, De Angelis C, Onori S and Cirrone G A P 2003 Diamond detector versus silicon diode and ion chamber in photon beams of different energy and field size *Med. Phys.* **30** 2149–54
Buonanno M, Grilj V and Brenner D J 2019 Biological effects in normal cells exposed to FLASH dose rate protons *Radiother. Oncol.* **139** 51–55
Burns D T and Mcewen M R 1998 Ion recombination corrections for the NACP parallel-plate chamber in a pulsed electron beam *Phys. Med. Biol.* **43** 2033–45
Busold S and Röcken H 2017 *21st Int. Conf. on Cyclotrons and Their Applications (Cyclotrons' 16)* (*Zurich, Switzerland, 11–16 September 2016*) vol Series (Geneva, Switzerland: JACOW) pp 313–5
Buttar C, Airey R, Conway J, Hill G, Ramkumar S, Scarsbrook G, Sussmann R, Walker S and Whitehead A 2000 A study of radiotherapy dosimeters based on diamond grown by chemical vapour deposition *Diam. Relat. Mater.* **9** 965–9
Castriconi R *et al* 2017 Dose-response of EBT3 radiochromic films to proton and carbon ion clinical beams *Phys. Med. Biol.* **62** 377–93
Cella L, Liuzzi R and Salvatore M 2010 The Italian affair: the employment of parallel-plate ionization chambers for dose measurements in high dose-per-pulse IORT electron beams *Med. Phys.* **37** 2918–24
Chalkley A and Heyes G 2014 Evaluation of a synthetic single-crystal diamond detector for relative dosimetry measurements on a CyberKnife™ *Br. J. Radiol.* **87** 20130768
Chen R and Leung P L 2001 Nonlinear dose dependence and dose-rate dependence of optically stimulated luminescence and thermoluminescence *Radiat. Meas.* **33** 475–81
Chen S N *et al* 2016 Absolute dosimetric characterization of Gafchromic EBT3 and HDv2 films using commercial flat-bed scanners and evaluation of the scanner response function variability *Rev. Sci. Instrum.* **87** 073301
Cherry Kemmerling E M, Wu M, Yang H, Maxim P G, Loo Jr B W and Fahrig R 2015 Optimization of an on-board imaging system for extremely rapid radiation therapy *Med. Phys.* **42** 6757–67
Cheung T, Butson M J and Yu P K N 2004 Experimental energy response verification of XR type T radiochromic film *Phys. Med. Biol.* **49** N371–6
Chiu C, Fomytskyi M, Grigsby F, Raischel F, Downer M C and Tajima T 2004 Laser electron accelerators for radiation medicine: a feasibility study *Med. Phys.* **31** 2042–52
Chung E, Bouchard H and Seuntjens J 2010 Investigation of three radiation detectors for accurate measurement of absorbed dose in nonstandard fields *Med. Phys.* **37** 2404–13
Ciancaglioni I, Marinelli M, Milani E, Prestopino G, Verona C, Verona-Rinati G, Consorti R, Petrucci A and De Notaristefani F 2012 Dosimetric characterization of a synthetic single crystal diamond detector in clinical radiation therapy small photon beams *Med. Phys.* **39** 4493–501
Cirrone G A P, Cuttone G, Raffaele L, Sabini M G, De Angelis C, Onori S, Pacilio M, Bucciolini M, Bruzzi M and Sciortino S 2003 Natural and CVD type diamond detectors as dosimeters in hadrontherapy applications *Nucl. Phys.* B **125** 179–83
Cottrell S S 2018 *Do Colors Exist?* (Berlin: Springer) pp 153–210
Crosbie J C, Fournier P, Bartzsch S, Donzelli M, Cornelius I, Stevenson A W, Requardt H and Bräuer-Krisch E 2015 Energy spectra considerations for synchrotron radiotherapy trials on the ID17 bio-medical beamline at the European synchrotron radiation facility *J. Synchrotron Radiat.* **22** 1035–41
Crosbie J C, Svalbe I, Midgley S M, Yagi N, Rogers P A W and Lewis R A 2008 A method of dosimetry for synchrotron microbeam radiation therapy using radiochromic films of different sensitivity *Phys. Med. Biol.* **53** 6861–77
Darafsheha A, Hao Y, Zwart T, Wagner M, Catanzano D, Williamson J F, Knutson N, Sun B, Mutic S and Zhao T 2020 Feasibility of proton FLASH irradiation using a synchrocyclotron for preclinical studies *Med. Phys.* (https://doi.org/10.1002/mp.14253)
Das T N, Ghanty T K and Pal H 2003 Reactions of methyl viologen dication (MV2+) with H atoms in aqueous solution: mechanism derived from pulse radiolysis measurements and ab initio MO calculations *J. Phys. Chem.* A **107** 5998–6006
Davis J A, Paino J R, Dipuglia A, Cameron M, Siegele R, Pastuovic Z, Petasecca M, Perevertaylo V L, Rosenfeld A B and Lerch M L F 2018 Characterisation and evaluation of a PNP strip detector for synchrotron microbeam radiation therapy *Biomed. Phys. Eng. Express* **4** 044002
Davis J A, Petasecca M, Cullen A, Paino J R, Archer J, Rosenfeld A B and Lerch M L F 2019 X-Tream dosimetry of synchrotron radiation with the PTW microDiamond *J. Instrum.* **14** P10037
Derikum K and Roos M 1993 Measurement of saturation correction factors of thimble-type ionization chambers in pulsed photon beams *Phys. Med. Biol.* **38** 755–63
Desrosiers M F, Puhl J M and Cooper S L 2008 An absorbed-dose/dose-rate dependence for the alanine-EPR dosimetry system and its implications in high-dose ionizing radiation metrology *J. Res. Natl Inst. Stand. Technol.* **113** 79–95
Devic S 2011 Radiochromic film dosimetry: past, present, and future *Phys. Medica* **27** 122–34
Di Martino F, Giannelli M, Traino A C and Lazzeri M 2005 Ion recombination correction for very high dose-per-pulse high-energy electron beams *Med. Phys.* **32** 2204–10
Di Venanzio C, Marinelli M, Tonnetti A, Verona-Rinati G, Falco M D, Pimpinella M, Ciccotelli A, De Stefano S, Felici G and Marangoni F 2015 Characterization of a microDiamond detector in high-dose-per-pulse electron beams for intra operative radiation therapy *Phys. Medica* **31** 897–902
Diffenderfer E S *et al* 2020 Design, implementation, and in vivo validation of a novel proton FLASH radiation therapy system *Int. J. Radiat. Oncol. Biol. Phys.* **106** 440–8
Dilmanian F A, Button T M, Le Duc G, Zhong N, Peña L A, Smith J A, Martinez S R, Bacarian T, Tammam J and Ren B 2002 Response of rat intracranial 9L gliosarcoma to microbeam radiation therapy *Neuro-Oncol.* **4** 26–38
Dilmanian F A, Krishnan S, Mclaughlin W E, Lukaniec B, Baker J T, Ailawadi S, Hirsch K N, Cattell R F, Roy R and Helfer J 2019 Merging orthovoltage x-ray minibeams spare the proximal tissues while producing a solid beam at the target *Sci. Rep.* **9** 1–15
Dilmanian F A, Morris G M, Zhong N, Bacarian T, Hainfeld J F, Kalef-Ezra J, Brewington L J, Tammam J and Rosen E M 2003 Murine EMT-6 carcinoma: high therapeutic efficacy of microbeam radiation therapy *Radiat. Res.* **159** 632–41
Dollinger G, Bergmaier A, Hable V, Hertenberger R, Greubel C, Hauptner A and Reichart P 2009 Nanosecond pulsed proton microbeam *Nucl. Instrum. Methods Phys. Res.* B **267** 2008–12

Doran S J, Rahman A T A, Bräuer-Krisch E, Brochard T, Adamovics J, Nisbet A and Bradley D 2013 Establishing the suitability of quantitative optical CT microscopy of PRESAGE® radiochromic dosimeters for the verification of synchrotron microbeam therapy *Phys. Med. Biol.* **58** 6279–97

Dowd R, Leblanc G and Zingre K 2008 Commissioning and operation of the 500 MHz storage ring RF system for the Australian synchrotron *Nucl. Instrum. Methods Phys. Res.* A **592** 224–9

Durante M, Bräuer-Krisch E and Hill M 2018 Faster and safer? FLASH ultra-high dose rate in radiotherapy *Br. J. Radiol.* **91** 20170628

Eduardo Villarreal-Barajas J and Khan R F H 2014 Energy response of EBT3 radiochromic films: implications for dosimetry in kilovoltage range *J. Appl. Clin. Med. Phys.* **15** 331–8

Epp E R, Weiss H, Djordjevic B and Santomasso A 1972 The radiosensitivity of cultured mammalian cells exposed to single high intensity pulses of electrons in various concentrations of oxygen *Radiat. Res.* **52** 324–32

Esplen N, Egoriti L, Gottberg A and Bazalova-Carter M 2019 Strategies for the delivery of spatially fractionated radiotherapy using conventional and FLASH-capable sources: scientific session 1: YIS–07 *Med. Phys.* **46** 5373

Faure J, Glinec Y, Pukhov A, Kiselev S, Gordienko S, Lefebvre E, Rousseau J P, Burgy F and Malka V 2004 A laser–plasma accelerator producing monoenergetic electron beams *Nature* **431** 541–4

Faure J, Rechatin C, Norlin A, Lifschitz A, Glinec Y and Malka V 2006 Controlled injection and acceleration of electrons in plasma wakefields by colliding laser pulses *Nature* **444** 737–9

Favaudon V, Caplier L, Monceau V, Pouzoulet F, Sayarath M, Fouillade C, Poupon M-F, Brito I, Hupé P and Bourhis J 2014 Ultrahigh dose-rate FLASH irradiation increases the differential response between normal and tumor tissue in mice *Sci. Transl. Med.* **6** 245ra93–ra93

Favaudon V, Lentz J-M, Heinrich S, Patriarca A, de Marzi L, Fouillade C and Dutreix M 2019 Time-resolved dosimetry of pulsed electron beams in very high dose-rate, FLASH irradiation for radiotherapy preclinical studies *Nucl. Instrum. Methods Phys. Res.* A **944** 162537

Favaudon V, Tourbez H, Houee-Levin C and Lhoste J M 1990 Carboxyl radical induced cleavage of disulfide bonds in proteins. A. gamma.-ray and pulse radiolysis mechanistic investigation *Biochemistry* **29** 10978–89

Fiorini F, Kirby D, Thompson J, Green S, Parker D J, Jones B and Hill M A 2014 Under-response correction for EBT3 films in the presence of proton spread out Bragg peaks *Phys. Medica* **30** 454–61

Fogh J, Fogh J M and Orfeo T 1977 One hundred and twenty-seven cultured human tumor cell lines producing tumors in nude mice *J. Natl Cancer Inst.* **59** 221–6

Fouillade C, Curras-Alonso S, Giuranno L, Quelennec E, Heinrich S, Bonnet-Boissinot S, Beddok A, Leboucher S, Karakurt H U and Bohec M 2020 FLASH irradiation spares lung progenitor cells and limits the incidence of radio-induced senescence *Clin. Cancer Res.* **26** 1497–506

Fournier P *et al* 2017 X-Tream dosimetry of highly brilliant X-ray microbeams in the MRT hutch of the Australian synchrotron *Radiat. Meas.* **106** 405–11

Fournier P, Crosbie J C, Cornelius I, Berkvens P, Donzelli M, Clavel A H, Rosenfeld A B, Petasecca M, Lerch M L F and Bräuer-Krisch E 2016 Absorbed dose-to-water protocol applied to synchrotron-generated x-rays at very high dose rates *Phys. Med. Biol.* **61** N349–N61

Franko A J and Sharplin J 1994 Development of fibrosis after lung irradiation in relation to inflammation and lung function in a mouse strain prone to fibrosis *Radiat. Res.* **140** 347–55

Geddes C G R, Toth C S, Van Tilborg J, Esarey E, Schroeder C B, Bruhwiler D, Nieter C, Cary J and Leemans W P 2004 A laser—plasma accelerator producing monoenergetic electron beams *Nature* **431** 538–41

Ghorbanpour Besheli M, Simiantonakis I, Zink K and Budach W 2016 Determination of the ion recombination correction factor for intraoperative electron beams *Z. Med. Phys.* **26** 35–44

Girdhani S, Abel E, Katsis A, Rodriquez A, Senapati S, Kuvillanueva A, Jackson I L, Eley J, Vujaskovic Z and Parry R 2019 Abstract LB-280: FLASH: a novel paradigm changing tumor irradiation platform that enhances therapeutic ratio by reducing normal tissue toxicity and activating immune pathways AACR

Glinec Y, Faure J, Malka V, Fuchs T, Szymanowski H and Oelfke U 2006 Radiotherapy with laser-plasma accelerators: Monte Carlo simulation of dose deposited by an experimental quasimonoenergetic electron beam *Med. Phys.* **33** 155–62

Glinec Y, Faure J, Pukhov A, Kiselev S, Gordienko S, Mercier B and Malka V 2005 Generation of quasi-monoenergetic electron beams using ultrashort and ultraintense laser pulses *Laser Part. Beams* **23** 161–6

Gomà C, Lorentini S, Meer D and Safai S 2014 Proton beam monitor chamber calibration *Phys. Med. Biol.* **59** 4961–71

Gomà C, Marinelli M, Safai S, Verona-Rinati G and Würfel J 2016 The role of a microDiamond detector in the dosimetry of proton pencil beams *Z. Med. Phys.* **26** 88–94

Gonzalez-Lopez A, Vera-Sanchez J-A and Lago-Martin J-D 2015 Small fields measurements with radiochromic films *J. Med. Phys.* **40** 61–67

Gotz M, Karsch L and Pawelke J 2017 A new model for volume recombination in plane-parallel chambers in pulsed fields of high dose-per-pulse *Phys. Med. Biol.* **62** 8634–54

Grams M P, Gustafson J M, Long K M and De Los Santos L E F 2015 Technical note: initial characterization of the new EBT-XD Gafchromic film *Med. Phys.* **42** 5782–6

Grilj V and Brenner D J 2018 LET dependent response of GafChromic films investigated with MeV ion beams *Phys. Med. Biol.* **63** 245021

Guénot D *et al* 2017 Relativistic electron beams driven by kHz single-cycle light pulses *Nat. Photon.* **11** 293–6

Guerda Massillon J L, Muñoz-Molina I D and Díaz-Aguirre P 2016 Optimum absorbed dose versus energy response of gafchromic EBT2 and EBT3 films exposed to 20–160 kV x-rays and 60Co gamma *Biomed. Phys. Eng. Express* **2** 045005

Gustas D, Guénot D, Vernier A, Dutt S, Böhle F, Lopez-Martens R, Lifschitz A and Faure J 2018 High-charge relativistic electron bunches from a kHz laser-plasma accelerator *Phys. Rev. Accel. Beams.* **21** 1–7

Hendry J H, Moore J V, Hodgson B W and Keene J P 1982 The constant low oxygen concentration in all the target cells for mouse tail radionecrosis *Radiat. Res.* **92** 172–81

Hill M A, Stevens D L, Marsden S J, Allott R, Turcu I C E and Goodhead D T 2002 Is the increased relative biological effectiveness of high LET particles due to spatial or temporal effects? Characterization and OER in V79-4 cells *Phys. Med. Biol.* **47** 3543–55

Hoban P W, Heydarian M, Beckham W A and Beddoe A H 1994 Dose rate dependence of a PTW diamond detector in the dosimetry of a 6 MV photon beam *Phys. Med. Biol.* **39** 1219–29

Hornsey S and Bewley D K 1972 Hypoxia in mouse intestine induced by electron irradiation at high dose-rates *Int. J. Radiat. Biol. Relat. Stud. Phys. Chem. Med.* **19** 479–83

ICRU 1982 *The Dosimetry of Pulsed Radiation* (Bethesda, MD: ICRU)

International Standardization Organization 2004 Standard practice for use of an alanine-EPR dosimetry system *Standard 51607: 2004 (E)*

Jaccard M, Durán M T, Petersson K, Germond J F, Liger P, Vozenin M C, Bourhis J, Bochud F and Bailat C 2018 High dose-per-pulse electron beam dosimetry: commissioning of the Oriatron eRT6 prototype linear accelerator for preclinical use *Med. Phys.* **45** 863–74

Jaccard M, Petersson K, Buchillier T, Germond J F, Durán M T, Vozenin M C, Bourhis J, Bochud F O and Bailat C 2017 High dose-per-pulse electron beam dosimetry: usability and dose-rate independence of EBT3 Gafchromic films *Med. Phys.* **44** 725–35

Jackson I L, Vujaskovic Z and Down J D 2010 Revisiting strain-related differences in radiation sensitivity of the mouse lung: recognizing and avoiding the confounding effects of pleural effusions *Radiat. Res.* **173** 10–20

Jackson J, Juang T, Adamovics J and Oldham M 2015 An investigation of PRESAGE® 3D dosimetry for IMRT and VMAT radiation therapy treatment verification *Phys. Med. Biol.* **60** 2217–30

Jaffé G 1913 Zur theorie der ionisation in Kolonnen *Ann. Phys.* **347** 303–44

Jorge P G *et al* 2019 Dosimetric and preparation procedures for irradiating biological models with pulsed electron beam at ultra-high dose-rate *Radiother. Oncol.* **139** 34–39

Kainz K K, Hogstrom K R, Antolak J A, Almond P R, Bloch C D, Chiu C, Fomytskyi M, Raischel F, Downer M and Tajima T 2004 Dose properties of a laser accelerated electron beam and prospects for clinical application *Med. Phys.* **31** 2053–67

Kamperis E, Kodona C and Giannouzakos V 2019 FLASH back to radiotherapy's past and then fast forward to the future *J. Cancer Prev. Curr. Res.* **10** 142–4

Karsch L 2016 Derivation of a formula describing the saturation correction of plane-parallel ionization chambers in pulsed fields with arbitrary repetition rate *Phys. Med. Biol.* **61** 3222–36

Karsch L, Beyreuther E, Burris-Mog T, Kraft S, Richter C, Zeil K and Pawelke J 2012 Dose rate dependence for different dosimeters and detectors: TLD, OSL, EBT films, and diamond detectors *Med. Phys.* **39** 2447–55

Karsch L, Beyreuther E, Enghardt W, Gotz M, Masood U, Schramm U, Zeil K and Pawelke J 2017 Towards ion beam therapy based on laser plasma accelerators *Acta Oncol.* **56** 1359–66

Karsch L, Richter C and Pawelke J 2011 Experimentelle Untersuchung der Sättigungskorrektion einer PTW Roos-Ionisationskammer in gepulsten Strahlungsfeldern mit hoher Pulsdosis bei verschiedenen Pulsdauern *Z. Med. Phys.* **21** 4–10

Karzmark C, White J and Fowler J 1964 Lithium fluoride thermoluminescence dosimetry *Phys. Med. Biol.* **9** 273

Khachonkham S, Dreindl R, Heilemann G, Lechner W, Fuchs H, Palmans H, Georg D and Kuess P 2018 Characteristic of EBT-XD and EBT3 radiochromic film dosimetry for photon and proton beams *Phys. Med. Biol.* **63** 065007

Kirby D, Green S, Palmans H, Hugtenburg R, Wojnecki C and Parker D 2010 LET dependence of GafChromic films and an ion chamber in low-energy proton dosimetry *Phys. Med. Biol.* **55** 417–33

Kirby-Smith J S and Dolphin G W 1958 Chromosome breakage at high radiation dose-rates *Nature* **182** 270–1

Kmetec J D, Gordon C L, Macklin J J, Lemoff B E, Brown G S and Harris S E 1992 MeV x-ray generation with a femtosecond laser *Phys. Rev. Lett.* **68** 1527–30

Koulouklidis A D, Cohen S and Kalef-Ezra J 2013 Thermochromic phase-transitions of GafChromic films studied by z-scan and temperature-dependent absorbance measurements *Med. Phys.* **40** 112701

Kry S, Popple R, Molineu A and Followill D 2012 SU-E-T-375: ion recombination correction factors (pion) for varian truebeam high dose rate therapy beams *Med. Phys.* **39** 3790–

Kudoh H, Celina M, Kaye R, Gillen K and Clough R 1997 Response of alanine dosimeters at very high dose rate *Appl. Radiat. Isot.* **48** 497–9

Laissue J A *et al* 2013 Response of the rat spinal cord to x-ray microbeams *Radiother. Oncol.* **106** 106–11

Laissue J A *et al* 1998 Neuropathology of ablation of rat gliosarcomas and contiguous brain tissues using a microplanar beam of synchrotron-wiggler-generated x rays *Int. J. Cancer* **78** 654–60

Laitano R F, Guerra A S, Pimpinella M, Caporali C and Petrucci A 2006 Charge collection efficiency in ionization chambers exposed to electron beams with high dose per pulse *Phys. Med. Biol.* **51** 6419–36

Lansonneur P, Favaudon V, Heinrich S, Fouillade C, Verrelle P and De Marzi L 2019 Simulation and experimental validation of a prototype electron beam linear accelerator for preclinical studies *Phys. Medica* **60** 50–57

Lárraga-Gutiérrez J M, Ballesteros-Zebadúa P, Rodríguez-Ponce M, García-Garduno O A and De La Cruz O O G 2015 Properties of a commercial PTW-60019 synthetic diamond detector for the dosimetry of small radiotherapy beams *Phys. Med. Biol.* **60** 905–24

Lempart M, Blad B, Adrian G, Bäck S, Knöös T, Ceberg C and Petersson K 2019 Modifying a clinical linear accelerator for delivery of ultra-high dose rate irradiation *Radiother. Oncol.* **139** 40–5

Lerch M L F, Petasecca M, Cullen A, Hamad A, Requardt H, Bräuer-Krisch E, Bravin A, Perevertaylo V L and Rosenfeld A B 2011 Dosimetry of intensive synchrotron microbeams *Radiat. Meas.* **46** 1560–5

Li Z, Wen D, Chen D, Peng S, Zhang L and Shi K 2000 A study of dosimetry characteristics of GAF DM-1260 radiochromic films *Radiat. Phys. Chem.* **57** 103–13

Liszka M, Stolarczyk L, Kłodowska M, Kozera A, Krzempek D, Mojzeszek N, Pędracka A, Waligórski M P R and Olko P 2018 Ion recombination and polarity correction factors for a plane-parallel ionization chamber in a proton scanning beam *Med. Phys.* **45** 391–401

Livingstone J *et al* 2017 Preclinical radiotherapy at the Australian synchrotron's imaging and medical beamline: instrumentation, dosimetry and a small-animal feasibility study *J. Synchrotron Radiat.* **24** 854–65

Livingstone J, Adam J F, Stevenson A W and Hausermann D 2016a Dosimetry for spatially fractionated synchrotron radiation therapy *Int. J. Radiat. Oncol. Biol. Phys.* **96** E658–E

Livingstone J, Stevenson A W, Butler D J, Häusermann D and Adam J F 2016b Characterization of a synthetic single crystal diamond detector for dosimetry in spatially fractionated synchrotron x-ray fields *Med. Phys.* **43** 4283–93

Loo B W, Schuler E, Lartey F M, Rafat M, King G J, Trovati S, Koong A C and Maxim P G 2017 (P003) delivery of ultra-rapid flash radiation therapy and demonstration of normal tissue sparing after abdominal irradiation of mice *Int. J. Radiat. Oncol. Biol. Phys.* **98** E16

Looe H K, Büsing I, Tekin T, Brant A, Delfs B, Poppinga D and Poppe B 2018 The polarity effect of compact ionization chambers used for small field dosimetry *Med. Phys.* **45** 5608–21

Lundh O, Rechatin C, Faure J, Ben-Ismaïl A, Lim J, De Wagter C, De Neve W and Malka V 2012 Comparison of measured with calculated dose distribution from a 120 MeV electron beam from a laser-plasma accelerator *Med. Phys.* **39** 3501–8

Lye J E, Harty P D, Butler D J, Crosbie J C, Livingstone J, Poole C M, Ramanathan G, Wright T and Stevenson A W 2016 Absolute dosimetry on a dynamically scanned sample for synchrotron radiotherapy using graphite calorimetry and ionization chambers *Phys. Med. Biol.* **61** 4201–22
Maine P, Strickland D, Bado P, Pessot M and Mourou G 1988 Generation of ultrahigh peak power pulses by chirped pulse amplification *IEEE J. Quantum. Electron.* **24** 398–403
Malka V, Faure J, Gauduel Y A, Lefebvre E, Rousse A and Phuoc K T 2008 Principles and applications of compact laser–plasma accelerators *Nat. Phys.* **4** 447–53
Mangles S P, Murphy C, Najmudin Z, Thomas A G R, Collier J, Dangor A E, Divall E, Foster P, Gallacher J and Hooker C 2004 Monoenergetic beams of relativistic electrons from intense laser–plasma interactions *Nature* **431** 535
Marsolat F, De Marzi L, Patriarca A, Nauraye C, Moignier C, Pomorski M, Moignau F, Heinrich S, Tromson D and Mazal A 2016 Dosimetric characteristics of four PTW microDiamond detectors in high-energy proton beams *Phys. Med. Biol.* **61** 6413–29
Martínez-Rovira I, Sempau J and Prezado Y 2012 Development and commissioning of a Monte Carlo photon beam model for the forthcoming clinical trials in microbeam radiation therapy *Med. Phys.* **39** 119–31
Martišíková M, Ackermann B and Jäkel O 2008 Analysis of uncertainties in Gafchromic® EBT film dosimetry of photon beams *Phys. Med. Biol.* **53** 7013–27
Maryanski M J, Gore J C, Kennan R P and Schulz R J 1993 NMR relaxation enhancement in gels polymerized and cross-linked by ionizing radiation: a new approach to 3D dosimetry by MRI *Magn. Reson. Imaging* **11** 253–8
Massillon-JL G, Cueva-Prócel D, Díaz-Aguirre P, Rodríguez-Ponce M and Herrera-Martínez F 2013 Dosimetry for small fields in stereotactic radiosurgery using Gafchromic MD-V2-55 film, TLD-100 and alanine dosimeters *PLoS One* **8** e63418
Maxim P G, Keall P and Cai J 2019a FLASH radiotherapy: newsflash or flash in the pan? *Med. Phys.* **46** 4287–90
Maxim P G, Tantawi S G and Loo B W 2019b PHASER: a platform for clinical translation of FLASH cancer radiotherapy *Radiother. Oncol.* **139** 28–33
Mazin S 2017 Method and apparatus for emission guided radiation therapy Google Patents
McErlean C M, Bräuer-Krisch E, Adamovics J and Doran S J 2016 Assessment of optical CT as a future QA tool for synchrotron x-ray microbeam therapy *Phys. Med. Biol.* **61** 320–37
McEwen M, Dewerd L, Ibbott G, Followill D, Rogers D W O, Seltzer S and Seuntjens J 2014 Addendum to the AAPM's TG-51 protocol for clinical reference dosimetry of high-energy photon beams *Med. Phys.* **41** 1–20
McKeown S R 2014 Defining normoxia, physoxia and hypoxia in tumours-implications for treatment response *Br. J. Radiol.* **87** 20130676
Michel P, Buettig H, Gabriel F, Helm M, Lehnert U, Schneider C, Schurig R, Seidel W, Stehr D and Teichert J 2006 *Proc. FEL* vol Series (Citeseer) p 488
Miura H, Ozawa S, Hosono F, Sumida N, Okazue T, Yamada K and Nagata Y 2016 Gafchromic EBT-XD film: dosimetry characterization in high-dose, volumetric-modulated arc therapy *J. Appl. Clin. Med. Phys.* **17** 312–22
Montay-Gruel P *et al* 2019 Long-term neurocognitive benefits of FLASH radiotherapy driven by reduced reactive oxygen species *Proc. Natl Acad. Sci. USA* **116** 10943–51
Montay-Gruel P *et al* 2018 X-rays can trigger the FLASH effect: ultra-high dose-rate synchrotron light source prevents normal brain injury after whole brain irradiation in mice *Radiother. Oncol.* **129** 582–8
Montay-Gruel P *et al* 2017 Irradiation in a flash: unique sparing of memory in mice after whole brain irradiation with dose rates above 100Gy/s *Radiother. Oncol.* **124** 365–9
Morales J E, Crowe S B, Hill R, Freeman N and Trapp J V 2014 Dosimetry of cone-defined stereotactic radiosurgery fields with a commercial synthetic diamond detector *Med. Phys.* **41** 1–6
Muir B R and Mcewen M R 2015 *Cham, 2015* vol Series ed D A Jaffray (Springer International Publishing) pp 767–70
Mukumoto N *et al* 2017 Sparing of tissue by using micro-slit-beam radiation therapy reduces neurotoxicity compared with broad-beam radiation therapy *J. Radiat. Res.* **58** 17–23
Nariyama N 2005 Responses of GafChromic films for distribution of extremely high doses from synchrotron radiation *Appl. Radiat. Isot.* **62** 693–7
Nias A, Swallow A, Keene J and Hodgson B 1970 Survival of HeLa cells from 10 nanosecond pulses of electrons *Int. J. Radiat. Biol. Relat. Stud. Phys. Chem. Med.* **17** 595–8
Niroomand-Rad A, Blackwell C R, Coursey B M, Gall K P, Galvin J M, Mclaughlin W L, Meigooni A S, Nath R, Rodgers J E and Soares C G 1998 Radiochromic film dosimetry: recommendations of AAPM radiation therapy committee task group 55 *Med. Phys.* **25** 2093–115
Nowais S A, Kacperek A, Brunt J N H, Adamovics J, Nisbet A and Doran S J 2010 An investigation of the response of the radiochromic dosimeter PRESAGE™ to irradiation by 62 MeV protons *J. Phys. Conf. Ser.* **250** 155–9
Ohno Y, Torikoshi M, Suzuki M, Umetani K, Imai Y, Uesugi K and Yagi N 2008 Dose distribution of a 125 keV mean energy microplanar x-ray beam for basic studies on microbeam radiotherapy *Med. Phys.* **35** 3252–8
Olko P, Marczewska B, Czopyk L, Czermak M A, Kłosowski M and Waligórski M P R 2006 New 2-D dosimetric technique for radiotherapy based on planar thermoluminescent detectors *Radiat. Prot. Dosim.* **118** 213–8
Palma B, Bazalova-Carter M, Hårdemark B, Hynning E, Qu B, Loo B W and Maxim P G 2016 Assessment of the quality of very high-energy electron radiotherapy planning *Radiother. Oncol.* **119** 154–8
Palmans H, Thomas R and Kacperek A 2006 Ion recombination correction in the Clatterbridge centre of oncology clinical proton beam *Phys. Med. Biol.* **51** 903–17
Palmer A L, Dimitriadis A, Nisbet A and Clark C H 2015 Evaluation of Gafchromic EBT-XD film, with comparison to EBT3 film, and application in high dose radiotherapy verification *Phys. Med. Biol.* **60** 8741–52
Papiez L, Desrosiers C and Moskvin V 2002 Very high energy electrons (50–250 MeV) and radiation therapy *Technol. Cancer Res. Treat.* **1** 105–10
Patriarca A *et al* 2018 Experimental set-up for FLASH proton irradiation of small animals using a clinical system *Int. J. Radiat. Oncol. Biol. Phys.* **102** 619–26
Petasecca M *et al* 2012 X-tream: a novel dosimetry system for synchrotron microbeam radiation therapy *J. Instrum.* **7** P07022
Petersson K, Jaccard M, Germond J F, Buchillier T, Bochud F, Bourhis J, Vozenin M C and Bailat C 2017 High dose-per-pulse electron beam dosimetry—a model to correct for the ion recombination in the advanced markus ionization chamber *Med. Phys.* **44** 1157–67
Petersson K, Jaccard M, Vozenin M C, Montay-Gruel P, Trompier F, Buchillier T, Germond J F, Bochud F, Bourhis J and Bailat C 2016 Dosimetry of ultra high dose rate irradiation for studies on the biological effect induced in normal brain and GBM *Radiother. Oncol.* **118** S84–S

Piermattei A, Delle Canne S, Azario L, Russo A, Fidanzio A, Miceli R, Soriani A, Orvieto A and Fantini M 2000 The saturation loss for plane parallel ionization chambers at high dose per pulse values *Phys. Med. Biol.* **45** 1869–83
Pimpinella M, Ciancaglioni I, Consorti R, Venanzio C D, Guerra A S, Petrucci A, Stravato A and Verona-Rinati G 2012 A synthetic diamond detector as transfer dosimeter for Dw measurements in photon beams with small field sizes *Metrologia* **49** S207–10
Pittman M, Ferré S, Rousseau J P, Notebaert L, Chambaret J P and Chériaux G 2002 Design and characterization of a near-diffraction-limited femtosecond 100-TW 10-Hz high-intensity laser system *Appl. Phys.* B **74** 529–35
Planche T 2019 ARIEL beamline parameters
Pommarel L, Vauzour B, Mégnin-Chanet F, Bayart E, Delmas O, Goudjil F, Nauraye C, Letellier V, Pouzoulet F and Schillaci F 2017 Spectral and spatial shaping of a laser-produced ion beam for radiation-biology experiments *Phys. Rev. Accel. Beams.* **20** 032801
Pratx G and Kapp D S 2019a A computational model of radiolytic oxygen depletion during FLASH irradiation and its effect on the oxygen enhancement ratio *Phys. Med. Biol.* **64** 185005
Pratx G and Kapp D S 2019b Ultra-high-dose-rate FLASH irradiation may spare hypoxic stem cell niches in normal tissues *Int. J. Radiat. Oncol. Biol. Phys.* **105** 190–2
Prempree T, Michelsen A and Merz T 1969 The repair time of chromosome breaks induced by pulsed x-rays on ultra-high dose-rate *Int. J. Radiat. Biol. Relat. Stud. Phys. Chem. Med.* **15** 571–4
Prezado Y, Martínez-Rovira I, Thengumpallil S and Deman P 2011a Dosimetry protocol for the preclinical trials in white-beam minibeam radiation therapy *Med. Phys.* **38** 5012–20
Prezado Y, Sarun S, Gil S, Deman P, Bouchet A and Le Duc G 2012 Increase of lifespan for glioma-bearing rats by using minibeam radiation therapy *J. Synchrotron Radiat.* **19** 60–65
Prezado Y, Vautrin M, Martínez-Rovira I, Bravin A, Estève F, Elleaume H, Berkvens P and Adam J F 2011b Dosimetry protocol for the forthcoming clinical trials in synchrotron stereotactic radiation therapy (SSRT) *Med. Phys.* **38** 1709–17
Ptaszkiewicz M, Braurer-Kirsch E, Klosowski M, Czopyk L and Olko P 2008 TLD dosimetry for microbeam radiation therapy at the European synchrotron radiation facility *Radiat. Meas.* **43** 990–3
Raaymakers B, Lagendijk J, Overweg J, Kok J, Raaijmakers A, Kerkhof E, Van der Put R, Meijsing I, Crijns S and Benedosso F 2009 Integrating a 1.5 T MRI scanner with a 6 MV accelerator: proof of concept *Phys. Med. Biol.* **54** N229
Rama N, Saha T, Shukla S, Goda C, Milewski D, Mascia A, Vatner R, Sengupta D, Katsis A and Abel E 2019 Improved tumor control through t-cell infiltration modulated by ultra-high dose rate proton FLASH using a clinical pencil beam scanning proton system *Int. J. Radiat. Oncol. Biol. Phys.* **105** S164–S5
Reinhardt S, Draxinger W, Schreiber J and Assmann W 2013 A pixel detector system for laser-accelerated ion detection *J. Instrum.* **8** P03008
Reinhardt S, Hillbrand M, Wilkens J J and Assmann W 2012 Comparison of Gafchromic EBT2 and EBT3 films for clinical photon and proton beams *Med. Phys.* **39** 5257–62
Richter C *et al* 2011 A dosimetric system for quantitative cell irradiation experiments with laser-accelerated protons *Phys. Med. Biol.* **56** 1529–43
Rigaud O, Fortunel N O, Vaigot P, Cadio E, Martin M T, Lundh O, Faure J, Rechatin C, Malka V and Gauduel Y A 2010 Exploring ultrashort high-energy electron-induced damage in human carcinoma cells *Cell Death Dis.* **1** e73–3
Rink A, Lewis D F, Varma S, Vitkin I A and Jaffray D A 2008 Temperature and hydration effects on absorbance spectra and radiation sensitivity of a radiochromic medium *Med. Phys.* **35** 4545–55
Rosenfeld A B 2006 Electronic dosimetry in radiation therapy *Radiat. Meas.* **41** 134–53
Rosenfeld A B, Lerch M L F, Kron T, Brauer-Krisch E, Bravin A, Holmes-Siedle A and Allen B J 2001 Feasibility study of online high-spatial-resolution MOSFET dosimetry in static and pulsed x-ray radiation fields *IEEE Trans. Nucl. Sci.* **48** 2061–8
Rosenfeld A B, Member S, Kaplan G I, Allen B J, Dilmanian A, Orion I, Ren B and Lerch M L F 1999 Mosfet dosimetry of an x-ray microbeam *IEEE Trans. Nucl. Sci.* **46** 1774–80
Rossomme S, Delor A, Lorentini S, Vidal M, Brons S, Jäkel O, Cirrone G, Vynckier S and Palmans H 2020 Three-voltage linear method to determine ion recombination in proton and light-ion beams *Phys. Med. Biol.* **65** 045015
Russo S, Mirandola A, Molinelli S, Mastella E, Vai A, Magro G, Mairani A, Boi D, Donetti M and Ciocca M 2017 Characterization of a commercial scintillation detector for 2-D dosimetry in scanned proton and carbon ion beams *Phys. Medica* **34** 48–54
Rustgi S N and Frye D M D 1995 Dosimetric characterization of radiosurgical beams with a diamond detector *Med. Phys.* **22** 2117–21
Sabatasso S, Laissue J A, Hlushchuk R, Graber W, Bravin A, Bräuer-Krisch E, Corde S, Blattmann H, Gruber G and Djonov V 2011 Microbeam radiation-induced tissue damage depends on the stage of vascular maturation *Int. J. Radiat. Oncol. Biol. Phys.* **80** 1522–32
Sakama M, Kanai T, Kase Y, Komori M, Fukumura A and Kohno T 2005 Responses of a diamond detector to high-LET charged particles *Phys. Med. Biol.* **50** 2275–89
Schmid T E *et al* 2011 The effectiveness of 20 MeV protons at nanosecond pulse lengths in producing chromosome aberrations in human-hamster hybrid cells *Radiat. Res.* **175** 719–27
Schnürer M, Kalashnikov M P, Nickles P V, Schlegel T, Sandner W, Demchenko N, Nolte R and Ambrosi P 1995 Hard x-ray emission from intense short pulse laser plasmas *Phys. Plasmas* **2** 3106–10
Schüler E, Eriksson K, Hynning E, Hancock S L, Hiniker S M, Bazalova-Carter M, Wong T, Le Q T, Loo Jr B W and Maxim P G 2017a Very high-energy electron (VHEE) beams in radiation therapy; treatment plan comparison between VHEE, VMAT, and PPBS *Med. Phys.* **44** 2544–55
Schüler E, Trovati S, King G, Lartey F, Rafat M, Villegas M, Praxel A J, Loo B W and Maxim P G 2017b Experimental platform for ultra-high dose rate FLASH irradiation of small animals using a clinical linear accelerator *Int. J. Radiat. Oncol. Biol. Phys.* **97** 195–203
Schulz R J, Nath R and Testa J R 1978 The effects of ultra-high dose rates on survival and sublethal repair in chinese-hamster cells *Int. J. Radiat. Biol.* **33** 81–88
Serduc R *et al* 2006 In vivo two-photon microscopy study of short-term effects of microbeam irradiation on normal mouse brain microvasculature *Int. J. Radiat. Oncol. Biol. Phys.* **64** 1519–27
Sharpe P H, Rajendran K and Sephton J P 1996 Progress towards an alanine/ESR therapy level reference dosimetry service at NPL *Appl. Radiat. Isot.* **47** 1171–5
Sharplin J and Franko A J 1989a A quantitative histological study of strain-dependent differences in the effects of irradiation on mouse lung during the early phase *Radiat. Res.* **119** 1–14
Sharplin J and Franko A J 1989b A quantitative histological study of strain-dependent differences in the effects of irradiation on mouse lung during the intermediate and late phases *Radiat. Res.* **119** 15–31

Shinohara K, Nakano H, Miyazaki N, Tago M and Kodama R 2004 Effects of single-pulse (⩽1 ps) X-rays from laser-produced plasmas on mammalian cells *J. Radiat. Res.* **45** 509–14
Shirato H, Suzuki K, Sharp G C, Fujita K, Onimaru R, Fujino M, Kato N, Osaka Y, Kinoshita R and Taguchi H 2006 Speed and amplitude of lung tumor motion precisely detected in four-dimensional setup and in real-time tumor-tracking radiotherapy *Int. J. Radiat. Oncol. Biol. Phys.* **64** 1229–36
Siegbahn E A, Bräuer-Krisch E, Bravin A, Nettelbeck H, Lerch M L F and Rosenfeld A B 2009 MOSFET dosimetry with high spatial resolution in intense synchrotron-generated x-ray microbeams *Med. Phys.* **36** 1128–37
Simmons D A *et al* 2019 Reduced cognitive deficits after FLASH irradiation of whole mouse brain are associated with less hippocampal dendritic spine loss and neuroinflammation *Radiother. Oncol.* **139** 4–10
Sipilä P, Ojala J, Kaijaluoto S, Jokelainen I and Kosunen A 2016 Gafchromic EBT3 film dosimetry in electron beams - energy dependence and improved film read-out *J. Appl. Clin. Med. Phys.* **17** 360–73
Skyt P S, Wahlstedt I, Muren L P, Petersen J B B and Balling P 2012 Temperature and temporal dependence of the optical response for a radiochromic dosimeter *Med. Phys.* **39** 7232–6
Slatkin D N, Spanne P, Dilmanian F A, Gebberst J O and Laissue J A 1995 Subacute neuropathological effects of microplanar beams of x-rays from a synchrotron wiggler *Med. Sci.* **92** 8783–7
Smyth L M, Donoghue J F, Ventura J A, Livingstone J, Bailey T, Day L R, Crosbie J C and Rogers P A 2018 Comparative toxicity of synchrotron and conventional radiation therapy based on total and partial body irradiation in a murine model *Sci. Rep.* **8** 12044
Sorriaux J, Kacperek A, Rossomme S, Lee J A, Bertrand D, Vynckier S and Sterpin E 2013 Evaluation of Gafchromic® EBT3 films characteristics in therapy photon, electron and proton beams *Phys. Medica* **29** 599–606
Spitz D R, Buettner G R, Petronek M S, St-Aubin J J, Flynn R T, Waldron T J and Limoli C L 2019 An integrated physico-chemical approach for explaining the differential impact of FLASH versus conventional dose rate irradiation on cancer and normal tissue responses *Radiother. Oncol.* **139** 23–7
Stevenson A W, Crosbie J C, Hall C J, Häusermann D, Livingstone J and Lye J E 2017 Quantitative characterization of the x-ray beam at the Australian synchrotron imaging and medical beamline (IMBL) *J. Synchrotron Radiat.* **24** 110–41
Strickland D and Mourou G 1985 Compression of amplified chirped optical pulses *Opt. Commun.* **56** 219–21
Subiel A *et al* 2014 Dosimetry of very high energy electrons (VHEE) for radiotherapy applications: using radiochromic film measurements and Monte Carlo simulations *Phys. Med. Biol.* **59** 5811–29
Sutton J D and Littler J P 2017 Accounting for the ion recombination factor in relative dosimetry of flattening filter free photon radiation *Biomed. Phys. Eng. Express* **3** 017002
Tajima H *et al* 2004 Performance of a low noise front-end ASIC for Si/CdTe detectors in compton gamma-ray telescope *IEEE Trans. Nucl. Sci.* **51** 842–7
Therriault-Proulx F, Beaulieu L, Archambault L and Beddar S 2013 On the nature of the light produced within PMMA optical light guides in scintillation fiber-optic dosimetry *Phys. Med. Biol.* **58** 2073
Tillman C, Grafström G, Jonsson A-C, Jönsson B-A, Mercer I, Mattsson S, Strand S-E and Svanberg S 1999 Survival of mammalian cells exposed to ultrahigh dose rates from a laser-produced plasma x-ray source *Radiology* **213** 860–5
Tochilin E and Goldstein N 1966 Dose rate and spectral measurements from pulsed x-ray generators *Health Phys.* **12** 1705–14
Todd P, Winchell H, Feola J and Jones G 1967 *Radiation Research* vol Series 31 Radiation Research Soc 2021 Spring RD, STE 600, Oak Brook, IL 60521 pp 644–&
Town C 1967 Effect of high dose rates on survival of mammalian cells *Nature* **215** 847–8
Uyama A, Kondoh T, Nariyama N, Umetani K, Fukumoto M, Shinohara K and Kohmura E 2011 A narrow microbeam is more effective for tumor growth suppression than a wide microbeam: an in vivo study using implanted human glioma cells *J. Synchrotron Radiat.* **18** 671–8
van de Water S, Safai S, Schippers J M, Weber D C and Lomax A J 2019 Towards FLASH proton therapy: the impact of treatment planning and machine characteristics on achievable dose rates *Acta Oncol.* **58** 1463–9
van Marlen P, Dahele M, Folkerts M, Abel E, Slotman B and Verbakel W 2019 Bringing FLASH to the clinic: treatment planning considerations for ultrahigh dose-rate proton beams *Int. J. Radiat. Oncol. Biol. Phys.* **106** 621–9
Venkatesulu B P, Sharma A, Pollard-Larkin J M, Sadagopan R, Symons J, Neri S, Singh P K, Tailor R, Lin S H and Krishnan S 2019 Ultra high dose rate (35 Gy/sec) radiation does not spare the normal tissue in cardiac and splenic models of lymphopenia and gastrointestinal syndrome *Sci. Rep.* **9** 1–9
Vozenin M C *et al* 2019a The advantage of FLASH radiotherapy confirmed in mini-pig and cat-cancer patients *Clin. Cancer Res.* **25** 35–42
Vozenin M C, Hendry J H and Limoli C L 2019b Biological benefits of ultra-high dose rate FLASH radiotherapy: sleeping beauty awoken *Clin. Oncol. (R. Coll. Radiol.)* **31** 407–15
Wang J, Trovati S, Borchard P M, Loo Jr B W, Maxim P G and Fahrig R 2017 Thermal limits on MV x-ray production by bremsstrahlung targets in the context of novel linear accelerators *Med. Phys.* **44** 6610–20
Wang Y, Easterling S B and Ting J Y 2012 Ion recombination corrections of ionization chambers in flattening filter-free photon radiation *J. Appl. Clin. Med. Phys.* **13** 262–8
Weinhous M S and Meli J A 1984 Determining Pion, the correction factor for recombination losses in an ionization chamber *Med. Phys.* **11** 846–9
Wilcox E E and Daskalov G M 2007 Evaluation of GAFCHROMIC® EBT film for CyberKnife® dosimetry *Med. Phys.* **34** 1967–74
Wilson J D, Hammond E M, Higgins G S and Petersson K 2020 Ultra-high dose rate (FLASH) radiotherapy: silver bullet or fool's gold? *Front. Oncol.* **9** 1563
Yogo A, Maeda T, Hori T, Sakaki H, Ogura K, Nishiuchi M, Sagisaka A, Kiriyama H, Okada H and Kanazawa S 2011 Measurement of relative biological effectiveness of protons in human cancer cells using a laser-driven quasimonoenergetic proton beamline *Appl. Phys. Lett.* **98** 053701
Yogo A, Sato K, Nishikino M, Mori M, Teshima T, Numasaki H, Murakami M, Demizu Y, Akagi S and Nagayama S 2009 Application of laser-accelerated protons to the demonstration of DNA double-strand breaks in human cancer cells *Appl. Phys. Lett.* **94** 181502
Zankowski C and Podgorsak E B 1998 Determination of saturation charge and collection efficiency for ionization chambers in continuous beams *Med. Phys.* **25** 908–15
Zeil K *et al* 2013 Dose-controlled irradiation of cancer cells with laser-accelerated proton pulses *Appl. Phys.* B **110** 437–44
Zlobinskaya O, Siebenwirth C, Greubel C, Hable V, Hertenberger R, Humble N, Reinhardt S, Michalski D, Röper B and Multhoff G 2014 The effects of ultra-high dose rate proton irradiation on growth delay in the treatment of human tumor xenografts in nude mice *Radiat. Res.* **181** 177–83